



NACA

0143415

TECH LIBRARY KAFB, NM

RESEARCH MEMORANDUM

PERFORMANCE CHARACTERISTICS AT MACH NUMBERS TO 2.0

OF VARIOUS TYPES OF SIDE INLETS MOUNTED ON

FUSELAGE OF PROPOSED SUPERSONIC AIRPLANE

I - TWO-DIMENSIONAL COMPRESSION-RAMP

INLETS WITH SEMICIRCULAR COWLS

By Alfred S. Valerino

Lewis Flight Propulsion Laboratory
Cleveland, Ohio

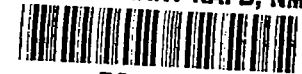
319.98/13



**NATIONAL ADVISORY COMMITTEE
FOR AERONAUTICS**

WASHINGTON
July 16, 1952

PERMANENT
RECORD
Resign signature required



1E

NACA RM E52E02

NATIONAL ADVISORY COMMITTEE FOR AERONAUTICS

RESEARCH MEMORANDUM

PERFORMANCE CHARACTERISTICS AT MACH NUMBERS TO 2.0 OF

VARIOUS TYPES OF SIDE INLETS MOUNTED ON FUSELAGE

OF PROPOSED SUPERSONIC AIRPLANE

I - TWO-DIMENSIONAL COMPRESSION-RAMP INLETS

WITH SEMICIRCULAR COWLS

By Alfred S. Valerino

SUMMARY

An experimental investigation was conducted to determine the performance of twin-scoop side inlets located on the fuselage of a proposed aircraft in a region of large boundary-layer thickness. Inlet configurations with subsonic and supersonic cowlings which utilized two-dimensional compression ramps and ram-type scoops for boundary-layer-removal systems were investigated at free-stream Mach numbers of 0, 0.63, and 1.5 to 2.0.

Significant gains in pressure recovery with a slight effect on drag were achieved by removing the entire boundary layer upstream of the inlets. The decrease in effective boundary-layer removal caused by the changes in the thickness of the boundary layer accounted for a large portion of the losses in total pressure at angles of attack.

Use of a sharp lip cowling penalized the pressure recoveries of the inlet at take-off and at a free-stream Mach number of 0.63. At free-stream Mach numbers of 1.5 and 2.0 and at an angle of attack of 3° , the increase in drag of the 14° ramp inlet with a rounded lip resulted in the equivalent of a 7 percent decrease in the ideal thrust of a typical engine.

INTRODUCTION

The pressure recoveries of side or aft inlets, which are usually located in a distorted flow field and in a region of boundary-layer air, have been considerably lower than those obtained with well-designed nose inlets (reference 1). The investigations reported in references 2 and 3 demonstrate that pressure recoveries comparable to those of

well-designed nose inlets could be obtained by the removal of all the boundary layer ahead of a half-conical spike inlet located in a uniform flow field. However, the application of these results to inlets located in a nonuniform flow field and to inlets other than the conical type has not been demonstrated.

A general side-inlet study was conducted in the NACA Lewis 8- by 6-foot supersonic tunnel to determine the aerodynamic characteristics of several types of supersonic side inlet with boundary-layer control mounted in a distorted flow field on a proposed airplane fuselage. A comparison of the performance of the inlet configurations investigated is summarized in reference 4. A detailed presentation of the results obtained from the study of semicircular cowl inlets with two-dimensional compression ramps is reported herein. The application of these results to the inlet-turbojet engine matching problem is discussed in reference 5.

The investigation was conducted through a range of angle of attack from 0° to 12° at Mach numbers of 0, 0.63, and 1.5 to 2.0. The Reynolds number, based on the length of the fuselage ahead of the inlets, was approximately 29×10^6 in the supersonic Mach number range. At a free-stream Mach number of 0.63, the corresponding Reynolds number was approximately 19×10^6 .

SYMBOLS

The following symbols are used in this report:

- A area
- C_D model forebody drag coefficient based on maximum body cross-sectional area of 1.784 sq ft
- D forebody drag
- F_n engine net thrust
- h height of boundary-layer ram scoop
- M Mach number
- m mass flow
- P total pressure
- P' pitot pressure

- p static pressure
 α angle of attack
 δ boundary-layer thickness

Subscripts:

- B boundary layer
c canopy survey station, station 67.5
cr critical
max maximum
p lip plus ramp projected area
s entrance to boundary-layer ram scoop
0 free stream
1 diffuser entrance station
2 diffuser discharge station

APPARATUS AND PROCEDURE

Several twin-scoop inlet configurations mounted on a one-fourth scale model of the forward portion of a fuselage of a supersonic aircraft were investigated. The inlet axes were canted down 2° with respect to the fuselage axis because of the estimated cross flow effects at cruising condition in flight, angle of attack of 3° . The inlets were located symmetrically about the vertical center line in the upper quadrants of the fuselage, aft of the oblique shock generated by the pilot's canopy. A photograph and a schematic diagram of the model, including representative cross sections, are presented in figures 1 and 2, respectively.

The semicircular scoop inlets reported herein utilized two-dimensional compression ramps for deceleration of the air and ram scoops, which spanned the inlets, for removal of the boundary-layer air. The air entering the twin inlets was diffused through two separate and identical ducts. The boundary-layer air likewise flowed through two separate and identical constant-area ducts which changed from a nearly rectangular cross section at the entrance to a circular

cross section at the exit (see fig. 2). Schematic diagrams of the inlets designed to operate at a flight Mach number of 2.0 are shown in figure 3. A notation system consisting of two numbers and a letter will be used herein for the discussion of these inlets: (1) an angle to designate the ramp angle, (2) an R or S to designate either a rounded subsonic cowl lip or a sharp supersonic cowl lip (figs. 3(b) and 3(c)), and (3) a number indicating the height, in inches, of the boundary-layer ram scoop. The letter O (for open) following the scoop height h indicates that approximately $2\frac{1}{2}$ inches of the sides of the ram scoops, aft of the leading edge of the ramp, were removed for inlets with a scoop height of 0.44 inch or that approximately 5 inches of the ram scoop sides were removed for inlets having a scoop height of 0.80 inch.

Inlets having ramp angles of 6° , 13° , and 14° were investigated. The inlet configuration 13°-R-0.44 shown in figure 3(d) was designed from subsonic considerations. Its ramp had an initial slope of 13° for a distance of 1 inch and then curved into the subsonic portion of the diffuser. The ramps of the other inlets were linear to the plane of the cowl lip. Inlets $14^\circ\text{-R-0.80(O)}$ and $14^\circ\text{-S-0.80(O)}$ shown in figures 3(f) and 3(g), respectively, had a scoop height of 0.80 inch which, due to model construction limitations, was obtained by moving the ramp leading edge forward 2.375 inches. The supersonic cowling of inlet $14^\circ\text{-S-0.80(O)}$ (fig. 3(g)) was moved forward $1\frac{1}{4}$ inches to intercept the oblique shock emanating from the leading edge of the ramp. A photograph of the $14^\circ\text{-S-0.80(O)}$ inlet is presented in figure 4.

The 14° and 6° ramps were used to simulate two positions of a variable-geometry type inlet (reference 5). The ramps were faired to the existing floor of the diffuser aft of station 74.75. The internal area variations of the inlets are presented in figure 5.

The mass flows through the inlets and the boundary-layer ducts were varied by means of remotely controlled plugs attached to the model sting. A three component strain-gage balance which measured the internal duct forces, fuselage drags, and model base forces, but not the forces acting on the plugs, was used to determine the drag characteristics. The drag presented is defined as the internal thrust developed, minus the strain-gage balance force, minus the base force. The thrust developed is the change in momentum of the air passing through the inlets from the free stream to the diffuser exit (station 97.25 of fig. 3(a)). Base forces were computed by obtaining the base area and the average base pressures from 13 static-pressure orifices located on the base of the model (section E-E of fig. 2).

Instrumentation in one of the two inlet ducts included 3 inlet rakes with 12 to 24 total-pressure tubes, located approximately 3 inches behind the cowl lip, from which the average total pressures at the entrance of the inlet were evaluated by an area weighting method. The diffuser discharge stations of both inlet ducts were instrumented with 8 wall static orifices and 8 radial rakes located at 45° intervals and consisting of 33 total-pressure tubes located at the centers of equal areas. The instrumentation at the exit of boundary-layer ducts consisted of 4 equally spaced radial rakes with 9 total-pressure tubes and 4 wall static orifices. The average total pressures at the diffuser and boundary-layer-duct discharge stations were also determined by an area weighting method and were used to calculate the mass flows based on a choked exit at the control plugs. The mass flow ratios of the inlets presented herein are based on the mass flows computed for the inlet duct with instrumentation at only the diffuser discharge station. Flow conditions upstream of the inlets (station 67.5) were surveyed by means of 5 wall static orifices and 5 removable rakes, each having 7 total-pressure tubes and each projecting 3 inches from the canopy surface.

The investigation at a Mach number of 0.63 was conducted by operating the tunnel subsonically. For simulating take-off conditions, inlet air was induced by attaching the model to the tunnel exhaust equipment.

Much of the experimental data were obtained at an angle of attack of 3° , which was selected as the cruise angle of attack of the model. Since the axes of the inlets were canted down 2° with respect to the fuselage axis, the inlets were at an angle of attack of 1° with respect to the free stream. A survey of the flow deflection approximately 1 inch upstream of the leading edge of the ramp indicated that the estimated average flow deflection angle for an angle of attack of 3° at a free-stream Mach number M_0 of 2.0 was $1^\circ 34'$ with respect to the inlet center line. The flow deflections were obtained by use of two wedge bars of 8° half angle, each having two impact tubes and two static-pressure orifices. Schematic diagrams of the wedge bar installation as well as a summary of the survey are shown in figure 6. The canopy Mach number M_c tabulated in figure 6 is the average Mach number obtained from the two total-pressure tubes and static-pressure orifices.

An additional survey of the flow conditions on the canopy at station 67.5 was conducted to determine the thickness of the boundary layer ahead of the inlets. The results of this study are presented in figure 7 as lines of constant total-pressure recoveries for M_0 of 2.0 and 1.5 at an angle of attack of 3° . The static pressures on the canopy surface were obtained with the canopy rakes removed and were assumed to be constant 3 inches from the canopy surface. Using

these static pressures and the measured pitot pressures, the canopy Mach numbers M_c were estimated and the pressure ratios P_c/P_0 were computed. The assumption of constant static pressures yielded pressure recoveries P_c/P_0 greater than unity outside the boundary layer. However, the boundary-layer thicknesses were not appreciably affected. The representative canopy Mach numbers M_c obtained from the survey are listed in the following table:

M_0	M_c
2.0	1.83
1.9	1.74
1.7	1.57
1.5	1.39

The boundary-layer thickness δ , which is indicated by the dashed line, was estimated to be 0.80 inch at M_0 of 2.0. This value of the boundary-layer thickness agrees closely with the approximation obtained from the flat-plate theory reported in reference 6.

The mass flow ratio, total-pressure recovery, and drag characteristics of the various inlets investigated were obtained at a constant bleed flow required for cooling purposes and equal to 0.1 of the rated flow of engine B discussed in reference 5. The bleed flow ratios reported herein are expressed as $(m_s/m_c)_B$, the ratio of the mass flow of boundary-layer air entering the ram scoop to that which could be handled by the ram scoop, based on the boundary-layer profiles obtained from the canopy survey and the area of the ram scoop.

For the range of diffuser discharge Mach number investigated, no pulsing was observed for any of the inlets.

DISCUSSION

Supersonic Mach Number Range

13°-R-0.44 inlet. - The aerodynamic characteristics of the 13°-R-0.44 inlet are presented in figure 8. Also presented in figure 8 are the constant bleed flow ratios $(m_s/m_c)_B$ as well as the maximum mass flows that could enter the inlet. These maximum mass flows were determined from the canopy flow conditions. The mass flow ratio $m_2/m_{0,p}$ is defined as the ratio of the mass flow passing through the inlet to the mass flow in a free-stream tube area equal to the sum of the lip and compression ramp projected areas.

Decreasing M_0 resulted in slight increases in minimum total drag coefficient. For any given M_0 , the drag increased as the inlet was operated subcritically, which was caused primarily by the additive drag. The pressure recoveries P_2/P_0 obtained were comparable to those of configuration B of reference 7, which was essentially a 1/20 scale version of the 13° -R-0.44 inlet tested in the Ames 8- by 8-inch supersonic tunnel. However, the pressure recoveries were considerably lower than those of well-designed nose inlets. These low recoveries were attributed to the boundary-layer air entering the inlet and to the reacceleration of the flow along the curved surface of the ramp.

14° -R-0.44 inlet. - To investigate the effect of the reacceleration of the flow ahead of the inlet, a linear 14° compression ramp was installed. The performance of the 14° -R-0.44 inlet is presented in figure 9. The minimum drags of the 14° -R-0.44 inlet were appreciably higher than those of the 13° -R-0.44 inlet. A comparison of the critical mass flows of the two inlets indicated approximately 15 percent more air spillage for the 14° ramp inlet and therefore an increase in additive drag. The higher spillage was associated with the increase in the internal contraction ratio from 1.10 to 1.21. Some internal contraction is inherent in the use of rounded lip inlets. The pressure recoveries at any M_2 near critical flow, however, were significantly improved for all M_0 but were still well below the values obtained from well-designed nose inlets.

Because the pressure recovery of a side inlet depends on the quantity of boundary layer removed ahead of the inlet (reference 2), the bleed flow of the 14° -R-0.44 inlet was varied while the position of the exit plug of the inlet was fixed at M_2 of 0.255. The variation of the inlet characteristics with bleed flow ratio $(m_s/m_c)_B$ at M_0 of 2.0 is presented in figure 10. Increasing the bleed flow ratio from 0.23 to 0.78 resulted in an increase in pressure recovery from 71 to 77 percent. The mass flow of the inlet also increased with increasing bleed flow while the total drag coefficient remained essentially constant. Because of the choking in the constant area duct, the ram scoop could operate at a maximum bleed flow ratio of only 0.78.

Since the increased bleed flow removal ahead of the inlet increased the pressure recovery of the inlet, the sides of the ram scoop of the 14° ramp inlet were removed so that the ram scoop could operate only at a bleed flow ratio $(m_s/m_c)_B$ of unity. Also, when the ram scoop sides were removed, the boundary-layer air not required for cooling was able to spill around and aft of the inlet. The corresponding changes of the air flow pattern into the ram scoops are shown in the schlieren photographs presented in figure 11. Removal of the sides eliminated the subcritical operation of the boundary-layer ducts shown in figure 11(a). The shock thickness in the photographs was caused by the fact that the inlets were skewed to the plane of the schlieren mirrors.

14°-R-0.44(0) inlet. - The performance of the 14°-R-0.44(0) inlet is presented in figure 12. Removal of the scoop sides slightly increased the pressure recoveries at all free-stream Mach numbers and also the mass flows of the inlet $m_2/m_{0,p}$. The drags, however, did not change significantly from those of the 14°-R-0.44 inlet.

14°-R-0.80(0) inlet. - In an attempt to improve the pressure recovery, the boundary-layer ram scoop height h was increased to 0.8 inch to obtain h/δ of 1.0, and the sides of the ram scoops were removed from the 14° ramp inlet so that $(m_s/m_c)_B = 1.0$. A schlieren photograph of the 14°-R-0.80(0) inlet (fig. 13) indicates that the entire boundary layer passed through the ram scoop. The characteristics of the 14°-R-0.80(0) inlet are presented in figure 14. A comparison with the 14°-R-0.44(0) inlet (fig. 12) indicates that at the critical flow condition comparable pressure recoveries were obtained at M_0 of 2.0, but that a slight gain was realized at M_0 of 1.5. In the sub-critical flow range, however, significant gains in pressure recovery were obtained with complete boundary-layer removal. The increase in the critical mass flows of approximately 6 percent at M_0 of 2.0 and 7 percent at M_0 of 1.5 over those of the 14°-R-0.44(0) inlet is associated with the decrease in the internal contraction ratio of the 14°-R-0.80(0) inlet. Increasing h/δ to 1.0, however, did not appreciably affect the minimum total drag coefficients.

A comparison of the characteristics of the 14°-R-0.80(0) inlet with those of the 13°-R-0.44 inlet (fig. 8) indicated that at critical flow conditions an approximate 10 percent gain in pressure recovery was obtained at M_0 of 2.0 at the cost of a 41 percent increase in total drag coefficient of the model.

6°-R-0.80(0) inlet. - A 6° ramp angle was selected to simulate the ramp position of a variable geometry turbojet inlet operating at M_0 of 1.5. Characteristics of the 6°-R-0.80(0) inlet with h/δ of 1.0 are shown in figure 15. A comparison of the 6°-R-0.80(0) inlet with the 14°-R-0.80(0) inlet (fig. 14) indicates that comparable peak pressure recoveries were obtained at M_0 of 1.5, but a higher peak pressure recovery was realized with the 14°-R-0.80(0) inlet at M_0 of 2.0. For critical flow conditions, a slightly higher recovery was obtained with the 6°-R-0.80(0) inlet at both M_0 of 1.5 and 2.0. The total drag coefficients of the 6°-R-0.80(0) inlet were considerably lower than those of the 14°-R-0.80(0) inlet because of the decrease in air spillage obtained with the lower internal contraction ratio of the 6°-R-0.80(0) inlet (fig. 5).

14°-S-0.80(0) inlet. - Since the drag with a subsonic lip is relatively high, the sharp lip inlet 14°-S-0.80(0) was designed and investigated to determine the magnitude of the drag penalty with a

subsonic lip inlet and the effect of the lip shape on the pressure recovery. The characteristics of the $14^\circ\text{-S-0.80(0)}$ inlet ($h/\delta = 1.0$) are presented in figure 16. For all the free-stream Mach numbers, pressure recoveries comparable to those of the $14^\circ\text{-R-0.80(0)}$ inlet (fig. 14) were obtained, but the total drag coefficients decreased to values slightly lower than those of the 6°-R-0.80(0) inlet (fig. 15). This decrease in drag was primarily caused by increasing the critical inlet mass flow by eliminating the internal contraction associated with the subsonic lip. Most of the air spillage obtained with the sharp lip inlet was due primarily to the two-dimensional ramp and shock configuration ahead of the three-dimensional semicircular cowl. However, a relatively small part of the spillage resulted from the flow detachment at the cowl lip. The spillage is shown qualitatively in the schlieren photograph presented in figure 17.

Thrust parameter. - To compare the inlets investigated, a thrust parameter $(F_n - D)/F_{n,ideal}$ can be selected for a particular installation. For this purpose, a turbojet engine (engine B of reference 5) operating in the tropopause and having pressure ratios of 1.42 and 1.87 at M_0 of 2.0 and 1.5, respectively, was selected as the power plant. The analysis assumes an afterburner temperature of 3900°R and a reexpanding nozzle and that the inlet and diffuser discharge areas could be adjusted to provide the necessary engine air flow at the required diffuser discharge Mach number.

The variation of the diffuser discharge Mach number M_2 with the thrust parameter $(F_n - D)/F_{n,ideal}$, which is defined as the ratio of the thrust developed by the engine at the experimentally determined pressure recoveries minus the forebody drag to the thrust developed by the engine at a pressure recovery of 1.0, is presented in figure 18. At M_0 of 1.5 and at an angle of attack of 3° , the lowest value of peak thrust parameter (0.618) was obtained with the installation utilizing the $14^\circ\text{-R-0.80(0)}$ inlet. Use of the $14^\circ\text{-S-0.80(0)}$ inlet-engine combination increased the peak value of the thrust parameter to 0.696, which was a $12\frac{1}{2}$ percent improvement over that of the $14^\circ\text{-R-0.80(0)}$ inlet installation. Since the pressure recoveries of the $14^\circ\text{-R-0.80(0)}$ and the $14^\circ\text{-S-0.80(0)}$ inlets were comparable, the gain in performance was attributed to the lower drag of the sharp lip inlet. This decrease in drag represents a 7 percent increase in the ideal engine thrust.

With the 6°-R-0.80(0) inlet-engine combination, the peak value of the thrust parameter was 0.691. However, a comparison of the performance of the 6°-R-0.80(0) inlet installation with those of the 14° ramp configurations should not be made on the basis of the data presented in figure 18(a) because of the significant change in drag which results by scaling the 14° ramp inlets to a size that would satisfy the breathing requirements of the engine operating at an M_0 of 1.5. This change in drag was not included in the data shown in figure 18(a).

~~CONFIDENTIAL~~

At M_0 of 2.0 (fig. 18(b)), the performances of the inlets improved considerably by increasing the boundary-layer removal. Included in figure 18(b) is the thrust parameter of the 13° ramp inlet with h/δ of 0 (designated 13°-R-0). The condition of $h = 0$ was obtained by the use of fairings from the canopy surface to the boundary-layer ram scoops. The lowest thrust minus drag was obtained with the 13°-R-0 inlet. The 13°-R-0.44 inlet installation improved the performance by approximately 17 percent. Changing the ramp angle to 14° resulted in an insignificant gain in peak thrust minus drag. In this case, the gain in thrust due to the increase in pressure recovery was approximately equal to the increase in spillage drag resulting from the higher internal contraction. Similarly, using the $14^\circ\text{-R-0.44(0)}$ inlet resulted in a negligible increase in performance over that of the 14°-R-0.44 inlet-engine combination. Use of the $14^\circ\text{-R-0.80(0)}$ inlet, however, resulted in a 21 percent increase in peak thrust minus drag over that of the 14°-R-0.44 inlet installation and a 24 percent gain over the 13°-R-0.44 inlet, thus indicating that the 41 percent increase in model drag is more than compensated for by the 10 percent gain in pressure recovery of the $14^\circ\text{-R-0.80(0)}$ inlet.

A comparison of the peak values of the thrust parameters of the $14^\circ\text{-R-0.80(0)}$, the 6°-R-0.80(0) , and the $14^\circ\text{-S-0.80(0)}$ inlet-engine combinations indicates that the $14^\circ\text{-S-0.80(0)}$ inlet installation performed approximately 15 percent and 9 percent better than did the $14^\circ\text{-R-0.80(0)}$ and the 6°-R-0.80(0) inlet installations, respectively. These improvements in performance are attributed to the lower drags of the $14^\circ\text{-S-0.80(0)}$ inlet. The decrease in drag of the sharp lip inlet represents a gain of 7 percent and 1 percent in ideal engine thrust over that of the $14^\circ\text{-R-0.80(0)}$ and the 6°-R-0.80(0) inlet-engine combinations, respectively. The thrust minus drag of the 6°-R-0.80(0) inlet installation was approximately 6 percent greater than that of the $14^\circ\text{-R-0.80(0)}$ inlet installation because of the lower additive drag of the 6° ramp inlet.

Breakdown of pressure losses. - Since the pressure recovery is relatively more important than the inlet drag in evaluating the performance of an inlet operating near the critical point, a breakdown of the flow process was made to determine where the pressure losses occurred. Figure 19 presents the variation with mass flow ratio at M_0 of 2.0 of the losses ahead of and behind the inlet measuring station for inlets having a subsonic cowl and for various amounts of boundary-layer removal. The mass flow ratio m_2/m_{critical} is the ratio of the mass flow entering the inlet to the critical mass flow of the inlet. The 13°-R-0 inlet had the highest entrance losses (fig. 19(a)) because of the high shock losses and zero boundary-layer removal. Increasing boundary-layer removal to h/δ of 0.55 decreased the entrance losses at m_2/m_{cr} of 0.95 from 0.36 to 0.255. Eliminating the reacceleration of the main stream by replacing the curved compression ramp with a linear 14° ramp

2481

~~CONFIDENTIAL~~

($h/\delta = 0.55$) reduced the entrance losses from 0.255 to 0.11. Removal of the entire boundary layer ahead of the 14° ramp inlet did not appreciably affect the losses at m_2/m_{cr} of 0.95. However, at lower mass flow ratios, a significant decrease in total-pressure losses was realized. Since the shock losses of the 6° ramp were higher than those of the 14° ramp, higher entrance losses were obtained with the 6° -R-0.80(0) inlet than with any of the 14° ramp inlets.

The losses aft of the inlet measuring station $\Delta P_{1-2}/P_0$, which are shown in figure 19(b), also decreased with increasing h/δ . By increasing h/δ from 0 to 0.55, the losses of the 13° ramp inlet at $m_2/m_{cr} = 0.95$ were reduced from 0.08 to 0.05. The losses of the 14° ramp inlet with h/δ of 0.55 were decreased from 0.17 to 0.14 by removing the sides of the ram scoop. Increasing h/δ to 1.0 resulted in a reduction of the losses to 0.06. The 6° -R-0.80(0) inlet experienced the least losses aft of the inlet measuring station. These losses, $\Delta P_{1-2}/P_0$, were apparently dependent on the geometry of the diffuser and the quantity of boundary-layer air entering the inlet.

The exit total-pressure contour maps of the inlets at a diffuser discharge Mach number M_2 near the peak thrust minus drag condition, which are presented in figure 20, show the nonuniform flow pattern at the diffuser discharge station. The high pressure regions for each inlet were found between the 1 o'clock and 3 o'clock positions, which correspond to that part of the inlet farthest from the body and the compression ramp. The low energy air was located in the region between the 4 o'clock and 10 o'clock positions and coincides with the surface which had the initial boundary layer and with the surface which had the greatest curvature in the subsonic diffuser (see fig. 3(a)). A low energy region existed for the conditions of complete boundary-layer removal ahead of the 14° -R-0.80(0) inlet (fig. 20(c)). A comparison of the high and low pressure regions in figure 20(c) illustrates the effect of curvature in the subsonic diffuser even though all surfaces had little or no boundary layer at the entrance of the inlet. However, the general level of the total pressures was appreciably higher for the condition of complete boundary-layer removal (fig. 20(c)) than for the condition of incomplete removal (fig. 20(b)).

Angle of Attack

The characteristics of the 14° -R-0.80(0) inlet at M_0 of 2.0 for the angle of attack range are presented in figure 21. The absolute values of the drag at angles of attack include the drag due to the fuselage normal force and as such are not directly applicable to the inlet except to indicate the magnitude of the additive drag at angles of attack. Figure 21 shows that the loss in pressure recovery from 0°

to 9° was slight. Increasing the angle of attack from 9° to 12° resulted in a large drop in pressure recovery. The other inlets investigated exhibited similar characteristics and the data are tabulated in table I.

An explanation of the insensitivity of the inlet pressure recovery at angles of attack up to 9° is provided by the pressure survey on the canopy ahead of the inlets. The results of the survey presented in figure 22 are plotted as contour lines of constant pitot pressure ratios and estimated boundary-layer thicknesses δ (dashed line) for the range of angle of attack at a free-stream Mach number of 2.0. The maximum boundary-layer thickness at 0° angle of attack was located at the bottom corner of the inlet. Increasing the angle of attack resulted in a shift of the maximum boundary-layer thickness to the top of the inlet because of the cross flow effects. However, the average boundary-layer thickness across the inlet did not increase significantly as the angle of attack was increased to 9° . Increasing the angle of attack to 12° resulted in a large increase in boundary-layer thickness and a breakdown of the flow at the top corner of the inlet. It appears that at an angle of attack of 12° the separation lobes reported in references 8 and 9 for bodies of revolution were definitely delayed for this fuselage shape because of the effective streamline cross section ahead of the inlets in the cross flow direction. It is therefore believed that the large decrease in pressure recovery from 9° to 12° angle of attack was associated with the effective decrease in h/δ_{\max} (reference 2).

The decrease in pressure recovery at angles of attack due to the decrease in effective boundary-layer removal has been estimated and is shown in figure 23 as the variation with angle of attack of the ratio of the pressure recovery at any angle of attack to the pressure recovery at an angle of attack of 3° . The reference curve, which represents the loss in pressure recovery due to incomplete removal of the boundary layer, was obtained from a plot of the effect of h/δ on the pressure recoveries of the 14° rounded lip inlets without ram scoop sides at an angle of attack of 3° and by estimating the effective h/δ_{\max} of the inlets at angles of attack, based on the data shown in figure 22. The recoveries used in figure 23 were those at the diffuser discharge Mach number obtained at an angle of attack of 3° for the peak thrust minus drag condition. The pressure recovery of the 14° -S-0.80(0) inlet was more sensitive to changes in angle of attack than was that of the 14° -R-0.80(0) inlet. It is also evident from figure 23 that at angles of attack, a large part of the losses in total-pressure recovery was due to the decrease in effective h/δ_{\max} .

The effect of angle of attack on the exit contour maps of the 14° -R-0.80(0) inlet is presented in figure 24. At 0° angle of attack, the high pressure region was found to exist at the outboard side of the inlet which was free of boundary-layer air. Increasing the angle of attack resulted in a movement of the high and low pressure fields in a

counterclockwise direction. At an angle of attack of 6° , the high and low energy regions were found essentially at the same locations as those at an angle of attack of 3° . At angles of attack of 9° and 12° , the low pressure fields were located in a region (between the 2 o'clock and the 9 o'clock positions) that corresponded to the bottom corner of the entrance section and the surface having the greatest curvature (fig. 3(a)).

Subsonic Mach Number of 0.63

The pressure recovery and mass flow characteristics of the $14^\circ\text{-S-0.80(0)}$ inlet at a free-stream Mach number of 0.63 are presented in figure 25. The maximum mass flow ratio of the inlet, 1.090, which is based on the minimum area of the inlet, is approximately 6 percent lower than that theoretically possible. The decrease in mass flow ratio is attributed to the effects of the vena contracta which forms at the lip of the inlet. As would be expected, high losses in pressure recovery occurred when the sharp lip inlet was operated at mass flow ratios greater than unity. These characteristics indicate that if the power plant used with this inlet requires mass flow ratios greater than 1.090, auxiliary intakes will be necessary to avoid severe performance penalties.

Static Conditions, Mach Number of 0

The $14^\circ\text{-R-0.80(0)}$, 6°-R-0.80(0) , and $14^\circ\text{-S-0.80(0)}$ inlets as well as a 6°-S-0.80(0) inlet were tested at M_0 of 0 to simulate the take-off conditions. The variation of the inlet pressure recovery with diffuser discharge Mach number is presented in figure 26. Higher pressure recoveries were obtained with the rounded-lip inlets than with the sharp-lip inlets. The pressure recoveries of the sharp-lip inlet also decreased faster with increasing M_2 than those of the rounded-lip inlets. As would be expected, the 6° ramp configurations had higher pressure recoveries than the 14° ramp inlets because of the lower entrance velocities of the 6° ramp inlets resulting from the larger minimum areas.

SUMMARY OF RESULTS

The results of the experimental investigation of side inlets with semicircular cowls utilizing two-dimensional compression ramps and boundary-layer removal and mounted in a distorted flow field on a proposed airplane fuselage are:

1. Increasing the amount of boundary-layer removal ahead of the 14° ramp inlets resulted in a substantial gain in pressure recovery with a slight effect on drag. With a typical engine operating at a free-stream Mach number of 2.0, the increase in pressure recovery of the 14° -R-0.80(0) inlet over that of the 14° -R-0.44 inlet represented a 21 percent gain in the thrust minus drag.

2. The change in boundary-layer thickness ahead of the compression ramp largely accounted for the loss in total pressure at angles of attack.

3. At an angle of attack of 3° and a free-stream Mach number of 2.0, an improvement was realized in the performance of the 14° -S-0.80(0) inlet over the performances of the 6° -R-0.80(0) and the 14° -R-0.80(0) inlets because the drags of the sharp lip inlet were lower than the drags of the rounded lip inlets, whereas the pressure recoveries of the three inlets were comparable. The higher drags of the rounded subsonic lip inlets resulted from the inherent internal contraction which caused excessive air spillage and a detached shock at the cowl lip. At a free-stream Mach number of 1.5, the increase in drag of the 14° -R-0.80(0) inlet penalized its performance. However, the rounded subsonic lip inlets performed much better than the sharp lip inlets at the take-off conditions.

Lewis Flight Propulsion Laboratory
National Advisory Committee for Aeronautics
Cleveland, Ohio

REFERENCES

1. Davis, Wallace F., Brajnikoff, George B., Goldstein, David I., and Spiegel, Joseph M.: An Experimental Investigation at Supersonic Speeds of Annular Duct Inlets Situated in a Region of Appreciable Boundary Layer. NACA RM A7G15, 1947.
2. Goelzer, H. Fred, and Cortright, Edgar M., Jr.: Investigation at Mach Number 1.88 of Half of a Conical-Spike Diffuser as a Side Inlet with Boundary-Layer Control. NACA RM E51G06, 1951.
3. Wittliff, Charles E., and Bryne, Robert W.: Preliminary Investigation of a Supersonic Scoop Inlet Derived from a Conical-Spike Nose Inlet. NACA RM L51G11, 1951.
4. Weinstein, M. I.: Performance of Supersonic Scoop Inlets. NACA RM E52A22, 1952.

5. Schueller, Carl F., and Esenwein, Fred T.: Analytical and Experimental Investigation of Inlet-Engine Matching for Turbojet-Powered Aircraft at Mach Numbers up to 2.0. NACA RM E51K20, 1952.
6. von Kármán, Th.: On Laminar and Turbulent Friction. NACA TM 1092, 1946.
7. Edwards, Sherman S.: Experimental Investigation at Supersonic Speeds of Scoops Employing Boundary-Layer Suction. NACA RM A9I29, 1949.
8. Luidens, Roger W., and Simon, Paul C.: Aerodynamic Characteristics of NACA RM-10 Missile in 8- by 6-Foot Supersonic Wind Tunnel at Mach Numbers from 1.49 to 1.98. I - Presentation and Analysis of Pressure Measurements (Stabilizing Fins Removed). NACA RM E50D10, 1950.
9. Allen, H. Julian, and Perkins, Edward W.: Characteristics of Flow over Inclined Bodies of Revolution. NACA RM A50L07, 1951.

TABLE I - AERODYNAMIC CHARACTERISTICS OF INLETS AT ANGLES OF ATTACK

Free-stream Mach number M_0 , 2.0																Free-stream Mach number M_0 , 1.5			
13°-R-0.44 inlet				14°-R-0.44 inlet				14°-R-0.44(0) inlet				14°-S-0.80(0) inlet				6°-R-0.80(0) inlet			
M_2	P_2/P_0	$m_2/m_{0,p}$	C_D	M_2	P_2/P_0	$m_2/m_{0,p}$	C_D	M_2	P_2/P_0	$m_2/m_{0,p}$	C_D	M_2	P_2/P_0	$m_2/m_{0,p}$	C_D	M_2	P_2/P_0	$m_2/m_{0,p}$	C_D
Angle of attack α , 0°																Angle of attack α , 0°			
0.468	0.625	0.833	0.0874	0.429	0.563	0.708	0.1125	0.429	0.570	0.731	0.1265	0.357	0.648	0.986	0.0834	0.465	0.749	0.752	0.1148
.327	.740	.737	.1189	.358	.648	.700	.1313	.358	.860	.729	.1434	.325	.700	.983	.0909	.429	.789	.745	.1166
.282	.784	.668	.1393	.326	.697	.696	.1518	.327	.708	.726	.1434	.282	.791	.957	.0950	.390	.847	.741	.1248
.255	.774	.617	.1539	.284	.758	.665	.1722	.285	.781	.708	.1388	.255	.858	.944	.1038	.358	.953	.736	.1300
.229	.779	.561	.1708	.254	.789	.629	.1905	.187	.839	.514	.1971	.228	.875	.868	.1207	.301	.965	.676	.1405
.188	.778	.465	.1970	.228	.817	.586	.1593	.149	.831	.407	.2264	.187	.866	.715	.1458	.267	.971	.610	.1574
				.188	.827	.494	.1908					.149	.860	.568	.1790	.220	.977	.512	.1778
				.149	.823	.394	.2235												
Angle of attack α , 3°																Angle of attack α , 3°			
0.466	0.606	0.806	0.0899	0.326	0.685	0.673	0.1230	0.429	0.559	0.719	0.1183	0.357	0.644	0.980	0.0857	0.465	0.748	0.751	0.1149
.391	.684	.794	.0979	.429	.548	.884	.1132	.358	.848	.716	.1347	.325	.692	.952	.0939	.390	.851	.744	.1288
.327	.715	.711	.1208	.359	.626	.678	.1260	.327	.686	.704	.1341	.282	.784	.951	.0950	.358	.955	.735	.1518
.292	.735	.643	.1416	.284	.721	.635	.1212	.283	.753	.680	.1308	.255	.835	.920	.1049	.301	.962	.674	.1434
.255	.741	.594	.1592	.254	.748	.596	.1354	.255	.773	.633	.1428	.241	.852	.892	.1125	.267	.969	.609	.1568
.188	.731	.456	.1957	.228	.762	.546	.1540	.229	.786	.581	.1603	.228	.865	.860	.1195	.220	.971	.508	.1778
				.188	.765	.458	.1831	.187	.788	.483	.1895	.187	.872	.719	.1458				
				.149	.754	.351	.2088	.149	.773	.379	.2145	.149	.862	.568	.1790				
Angle of attack α , 6°																Angle of attack α , 6°			
0.466	0.606	0.807	0.1080	0.429	0.537	0.672	0.1299	0.358	0.648	0.715	0.1498	0.357	0.643	0.954	0.0991	0.390	0.852	0.744	0.1458
.391	.666	.773	.1125	.358	.624	.674	.1440	.327	.694	.712	.1487	.325	.690	.950	.1020	.336	.951	.732	.1481
.327	.700	.696	.1311	.326	.665	.664	.1445	.283	.749	.676	.1458	.282	.772	.935	.1080	.301	.961	.672	.1568
.255	.735	.586	.1655	.284	.717	.632	.1428	.255	.770	.631	.1562	.255	.815	.900	.1169	.267	.968	.608	.1726
.229	.741	.533	.1818	.254	.746	.596	.1558	.229	.791	.585	.1714	.228	.849	.844	.1355	.220	.973	.509	.1941
.188	.739	.441	.2068	.228	.769	.553	.1749	.187	.805	.494	.2017	.187	.871	.719	.1597				
				.188	.784	.468	.2062	.149	.787	.385	.2250	.149	.865	.571	.1906				
				.149	.776	.372	.2367												
Angle of attack α , 9°																Angle of attack α , 9°			
0.468	0.597	0.782	0.1288	0.429	0.517	0.646	0.1562	0.429	0.545	0.702	0.1597	0.357	0.639	0.950	0.1288	0.390	0.847	0.740	0.1720
.391	.627	.728	.1346	.358	.606	.654	.1731	.358	.631	.699	.1737	.325	.681	.936	.1288	.336	.942	.724	.1871
.327	.659	.686	.1527	.326	.640	.639	.1678	.327	.677	.694	.1714	.282	.756	.915	.1376	.301	.956	.689	.1877
.255	.681	.542	.1875	.284	.690	.606	.1696	.283	.733	.661	.1768	.255	.798	.881	.1481	.267	.963	.605	.2017
.229	.687	.494	.2027	.254	.713	.588	.1819	.255	.751	.614	.1819	.228	.823	.818	.1615	.220	.967	.506	.2245
.204	.692	.447	.2156	.228	.731	.525	.1994	.229	.767	.665	.1959	.187	.844	.697	.1877				
				.188	.744	.445	.1743	.187	.781	.479	.2233	.149	.867	.572	.2169				
Angle of attack α , 12°																Angle of attack α , 12°			
0.468	0.551	0.734	0.1643	0.429	0.480	0.601	0.2005	0.429	0.494	0.634	0.1947	0.357	0.593	0.882	0.1533	0.390	0.833	0.728	0.2134
.391	.583	.878	.1660	.358	.559	.604	.2012	.358	.588	.649	.2070	.325	.641	.881	.1568	.336	.914	.704	.2163
.327	.601	.598	.1870	.326	.598	.596	.1954	.327	.624	.638	.2017	.282	.700	.848	.1697	.301	.939	.658	.2285
.255	.594	.473	.2138	.284	.639	.563	.2084	.283	.678	.611	.2084	.255	.729	.804	.1831	.267	.944	.594	.2443
.233	.590	.433	.2220	.254	.655	.522	.2200	.255	.687	.562	.2186	.228	.750	.745	.1936	.220	.941	.493	.2641
				.228	.680	.474	.2303	.229	.682	.504	.2326	.187	.767	.632	.2163	.364	.876	.723	.2134
				.188	.649	.388	.2472	.187	.664	.406	.2513	.149	.773	.510	.2408				

NACA

2481

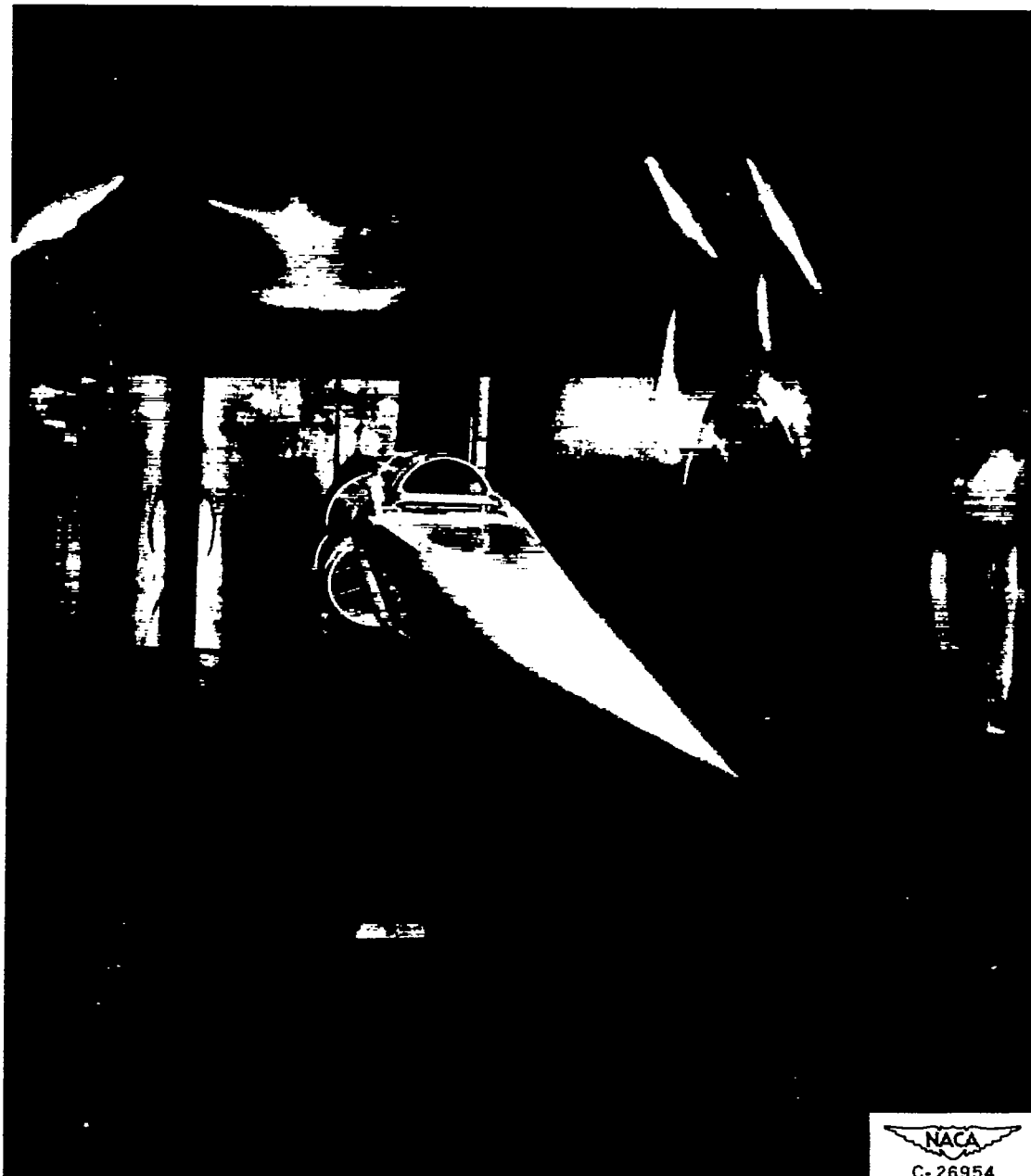


Figure 1. - Photograph of model rotated 56° .

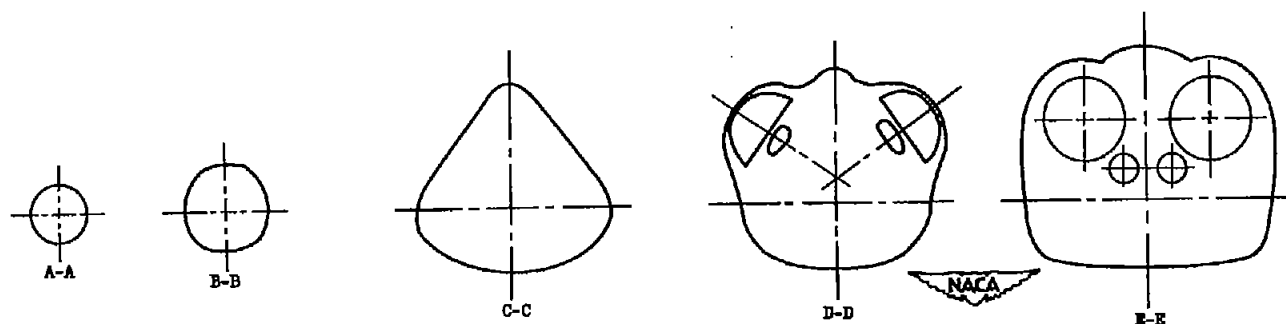
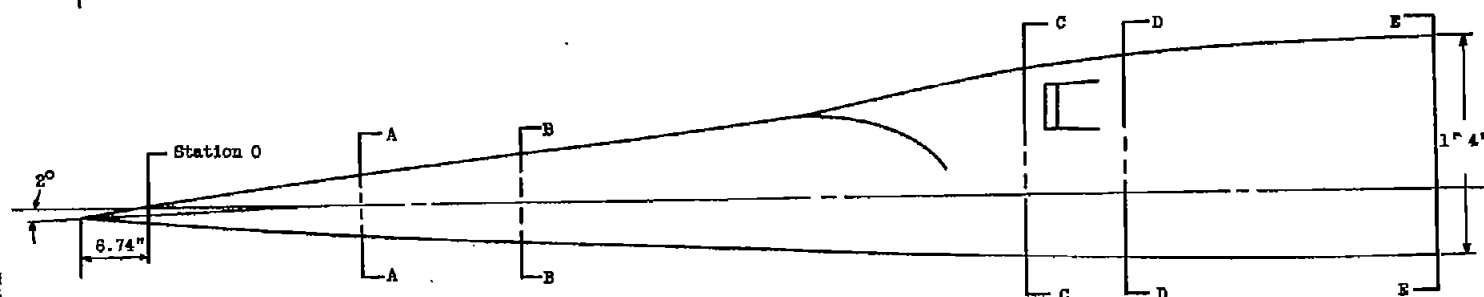
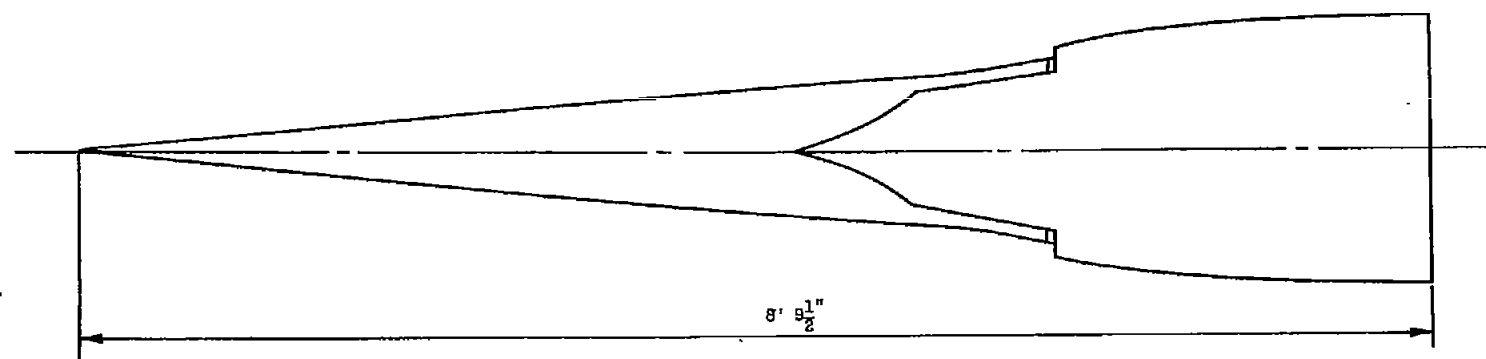
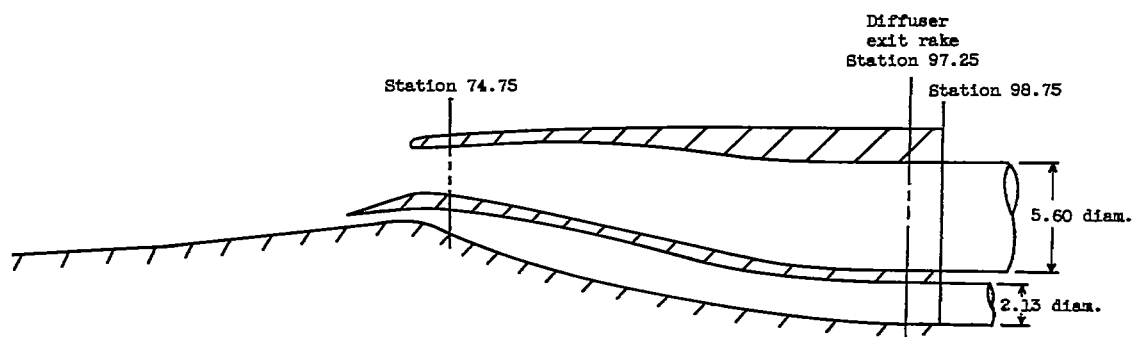
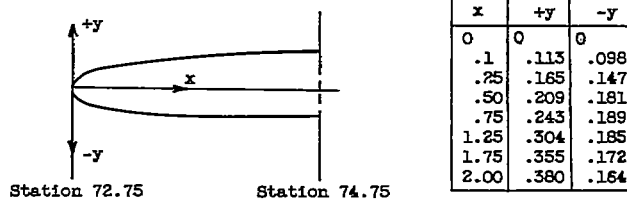


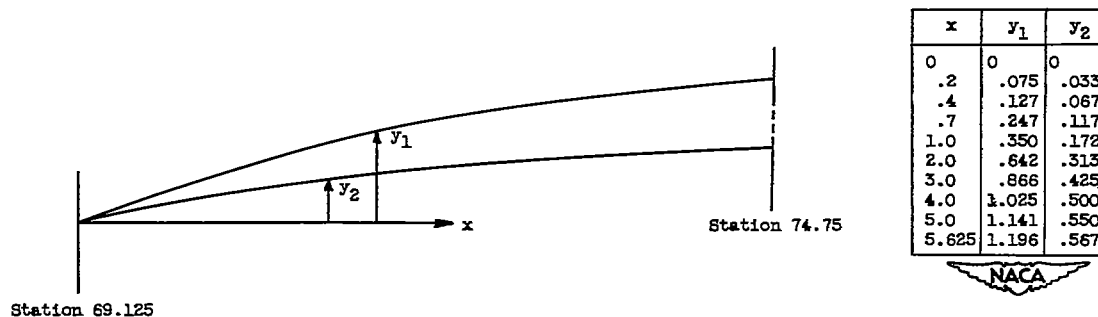
Figure 2. - Schematic diagram of model with representative cross sections.



(a) Cross-sectional view of inlet.



(b) Rounded subsonic cowl lip.



(c) Sharp supersonic cowl lip.

Figure 3. - Inlet configurations designed to operate at free-stream Mach number of 2.0.
(All dimensions are in inches.)

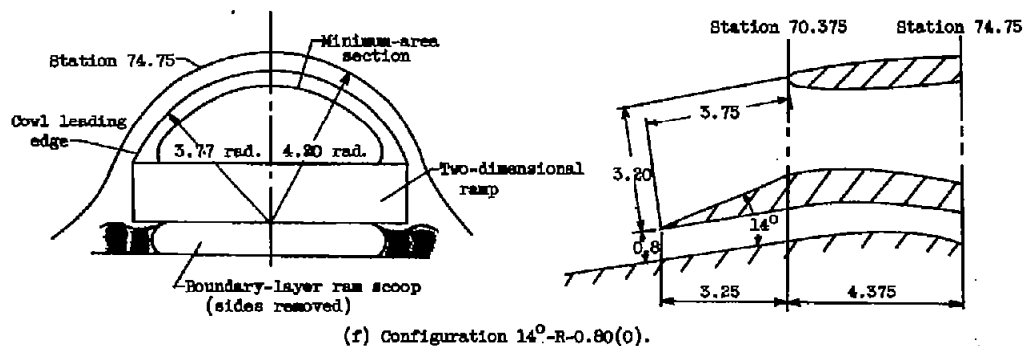
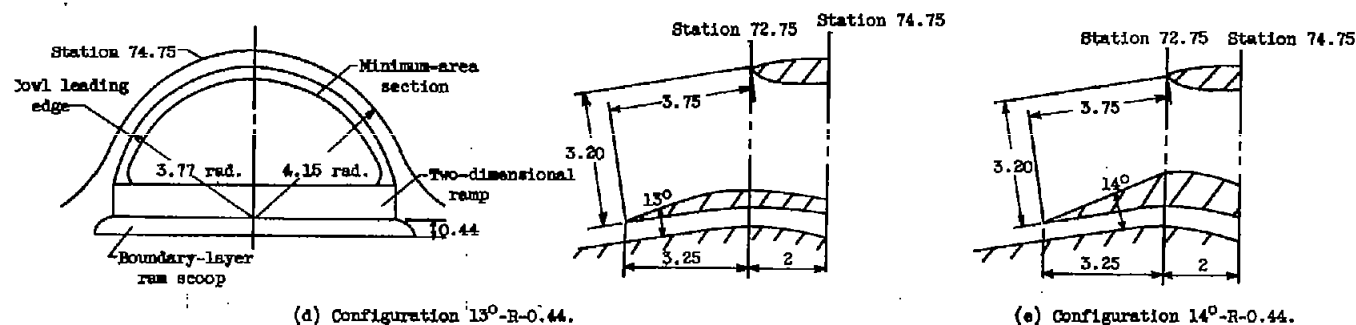


Figure 3. - Concluded. Inlet configurations designed to operate at free-stream Mach number of 2.0.
(All dimensions are in inches.)

2481

NACA RM E52E02

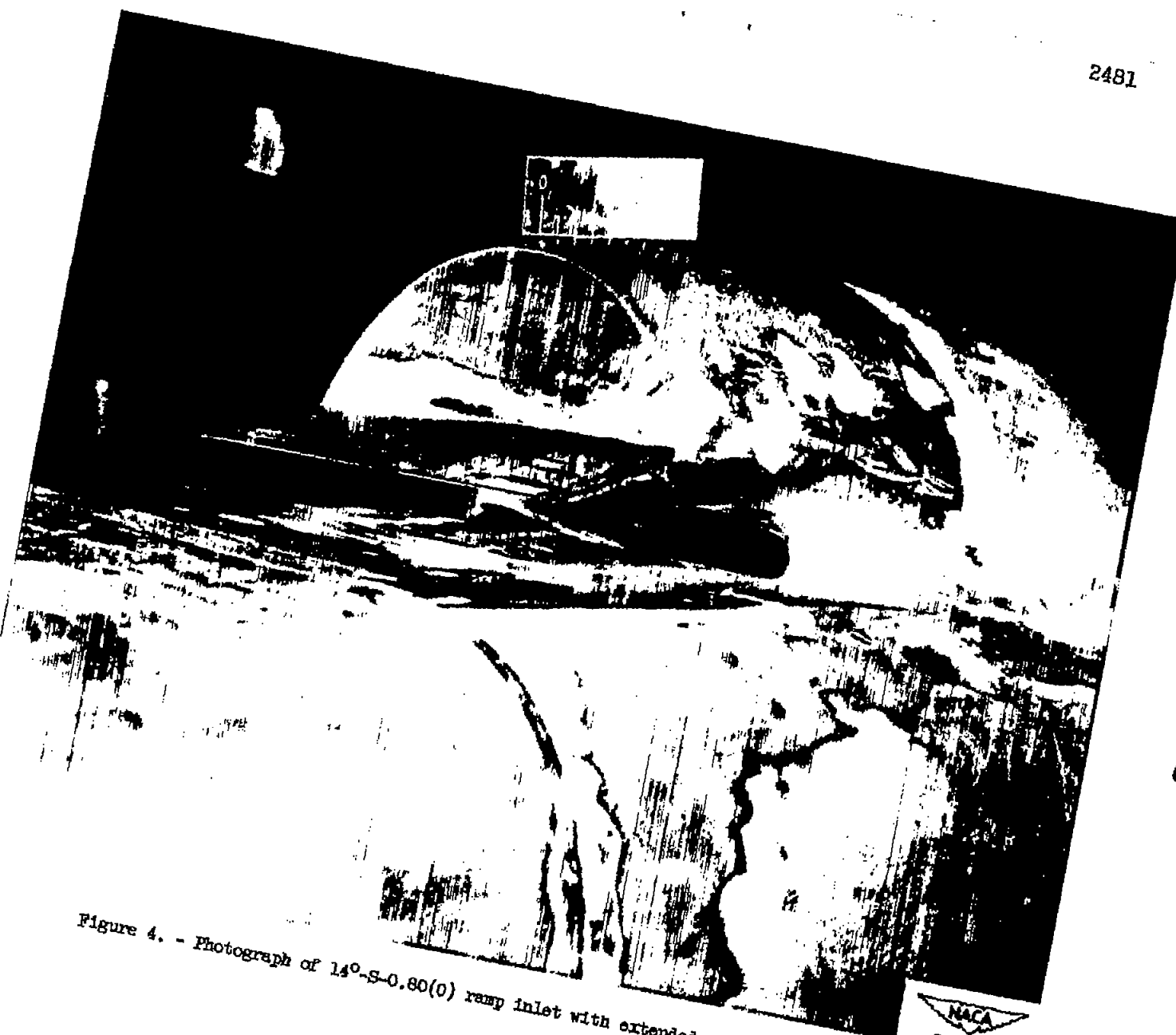


Figure 4. - Photograph of 14° -S-0.80(0) ramp inlet with extended supersonic cowling.

NACA
C-27538

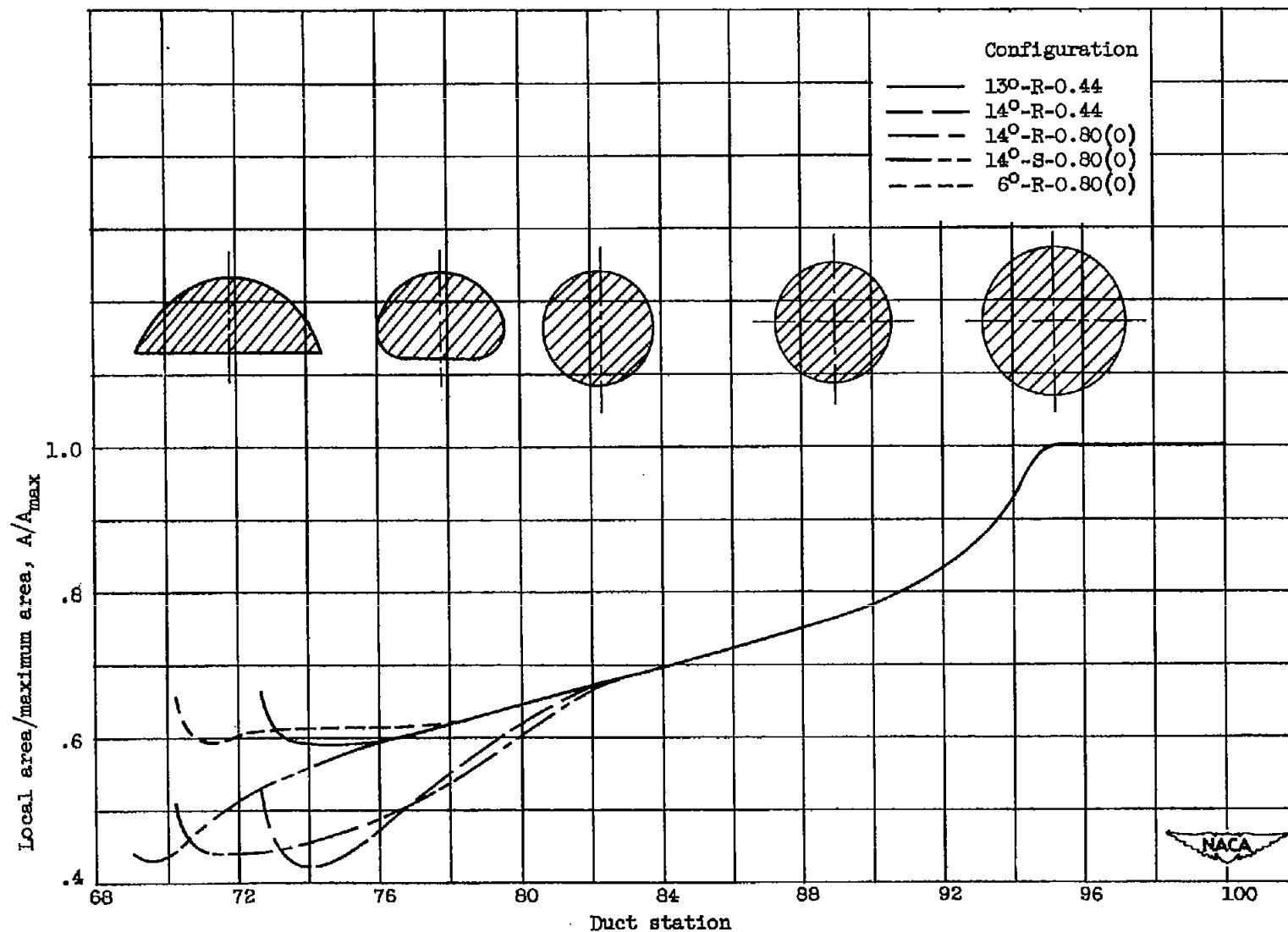


Figure 5. - Area variations of inlet configurations.

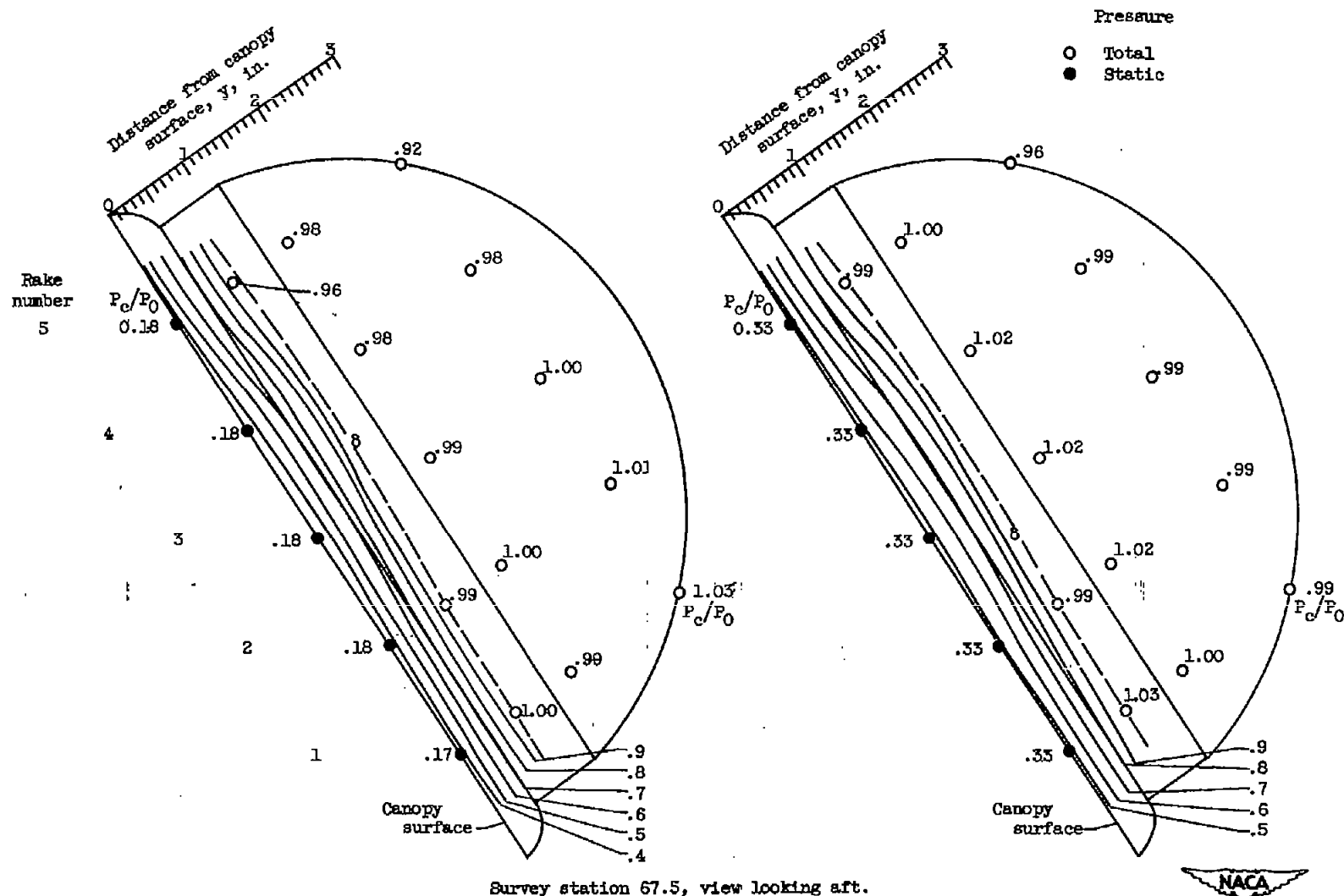


Figure 7. - Total-pressure survey upstream of inlets at angle of attack of 3° .

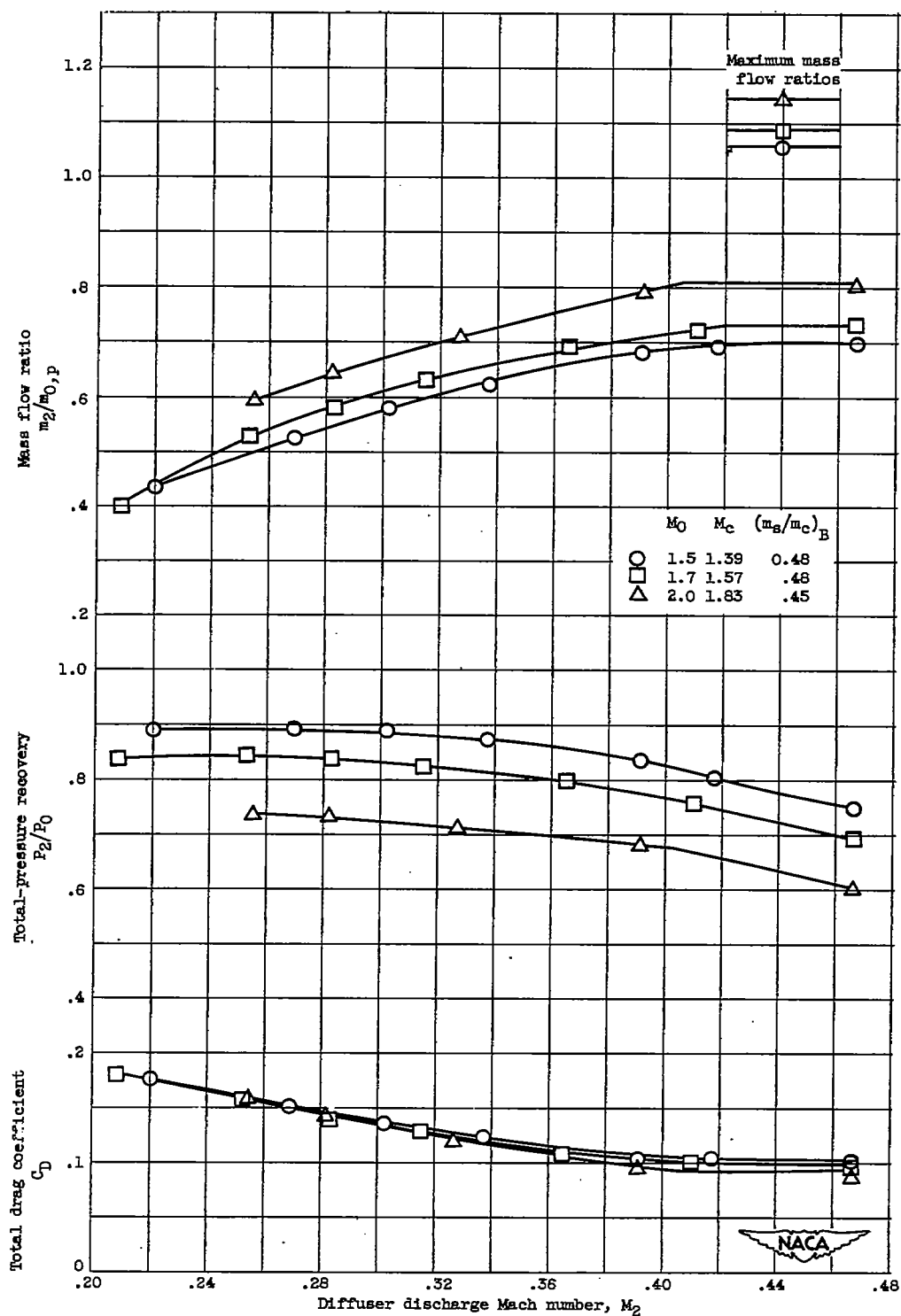


Figure 8. - Aerodynamic characteristics of 13°-R-0.44 inlet for range of free-stream Mach number at angle of attack of 3°.

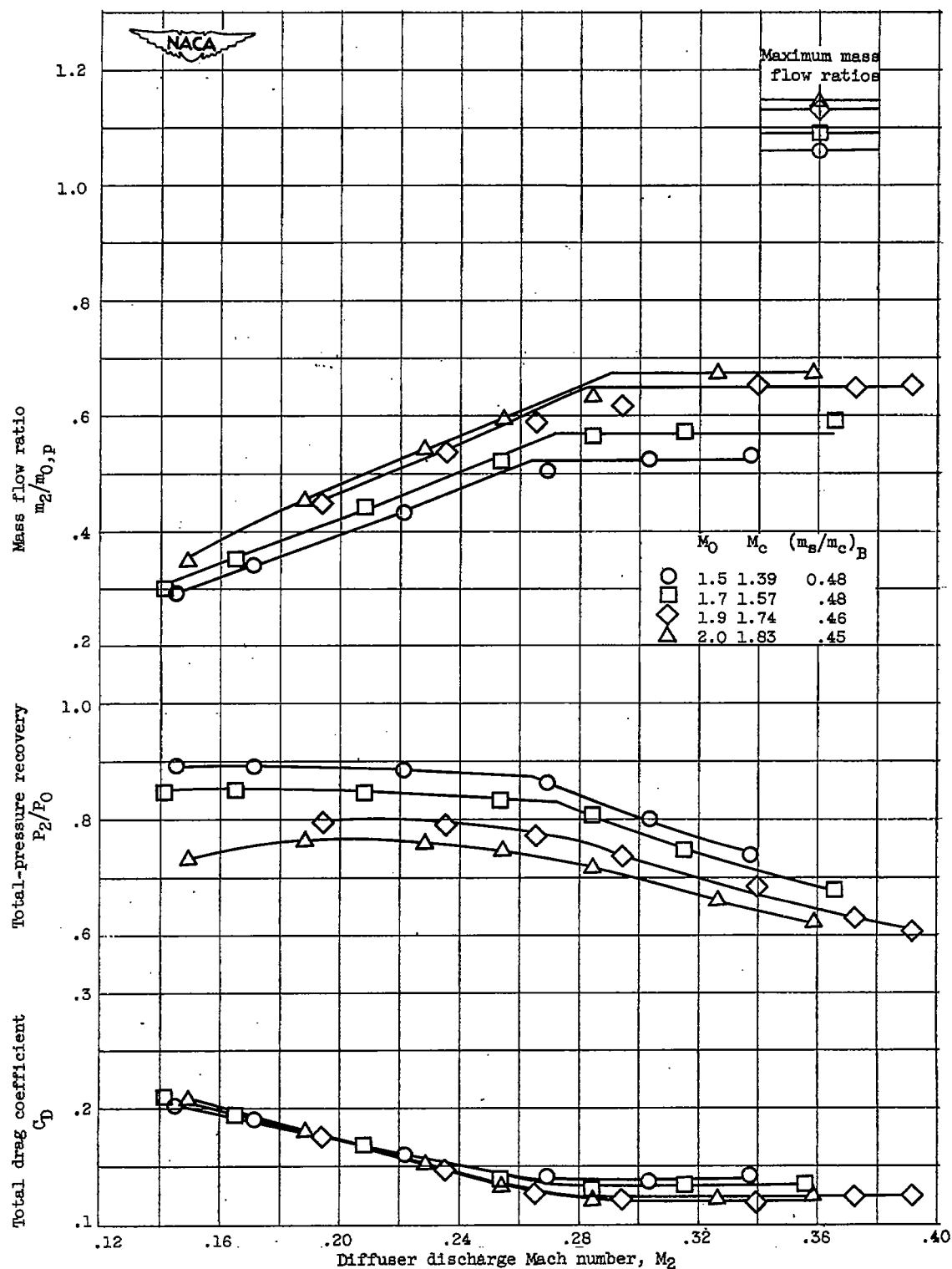


Figure 9. - Aerodynamic characteristics of 14°-R-0.44 inlet for range of free-stream Mach number at angle of attack of 3°.

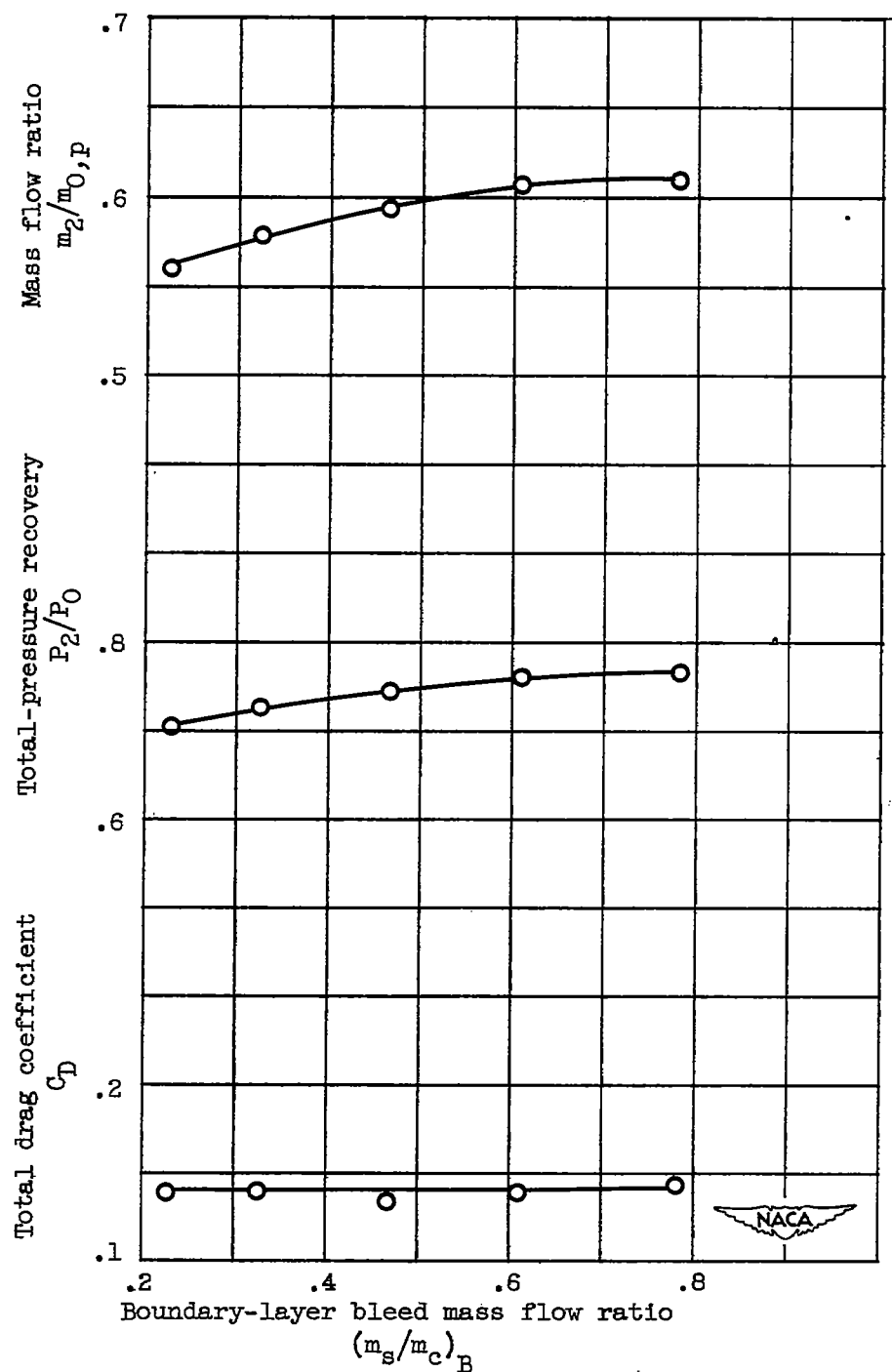
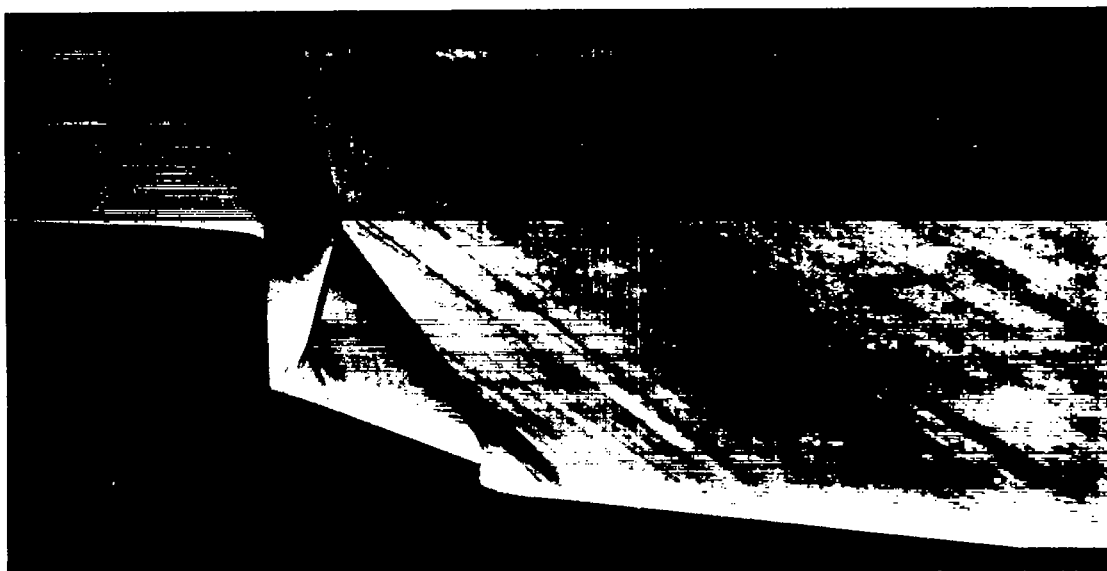


Figure 10. - Effect of bleed flow on aerodynamic characteristics of 14° -R-0.44 inlet at angle of attack of 3° and free-stream Mach number of 2.0. Diffuser discharge Mach number, 0.255.



(a) 14° -R-0.44 inlet



(b) 14° -R-0.44(0) inlet.

NACA
C-28984

Figure 11. - Schlieren photographs of 14° rounded lip inlets at free-stream Mach number of 2.0 and angle of attack of 3° . Diffuser discharge Mach number, 0.255.

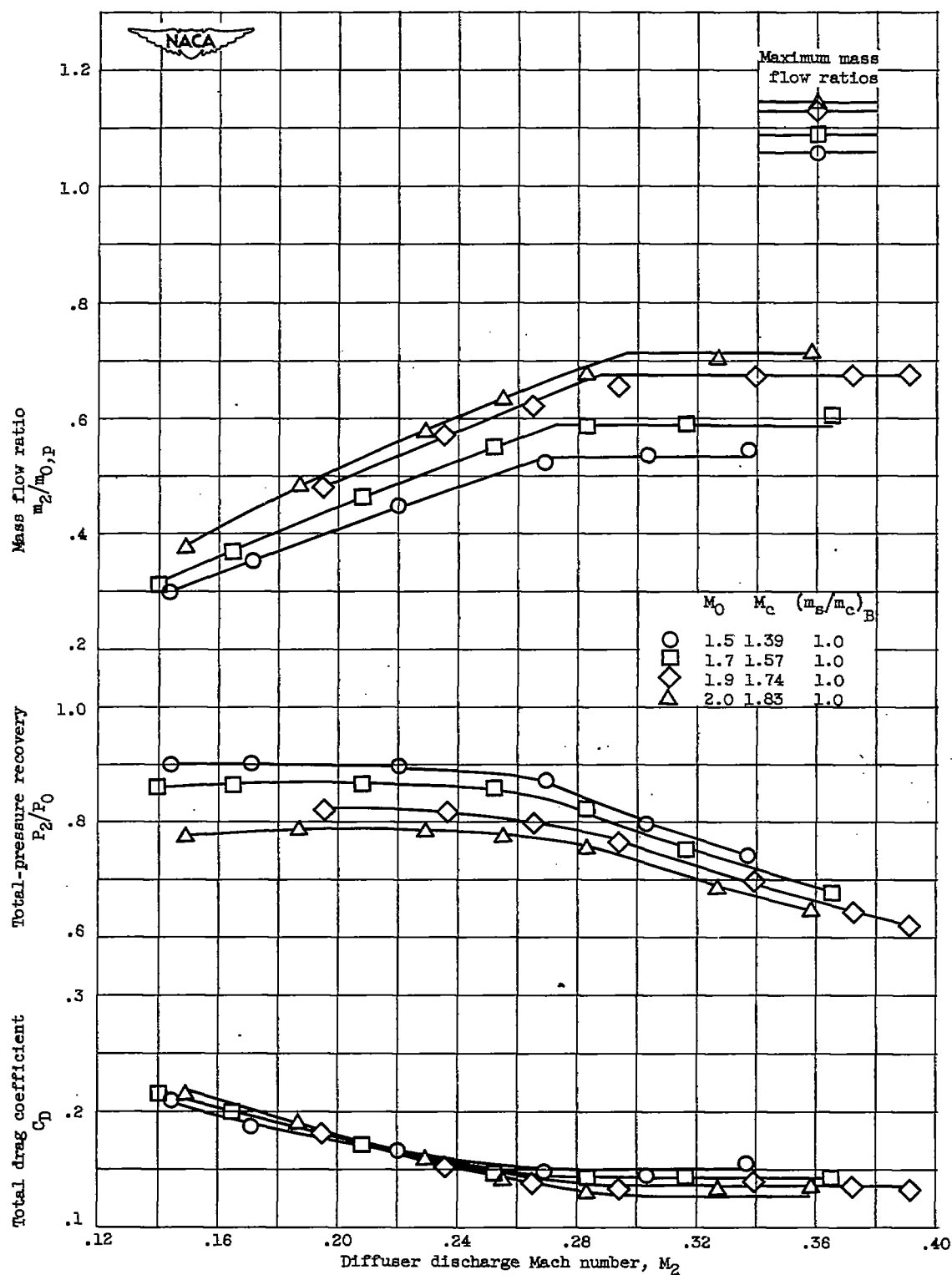


Figure 12. - Aerodynamic characteristics of 14°-R-0.44(0) inlet for range of free-stream Mach number at angle of attack of 3°.

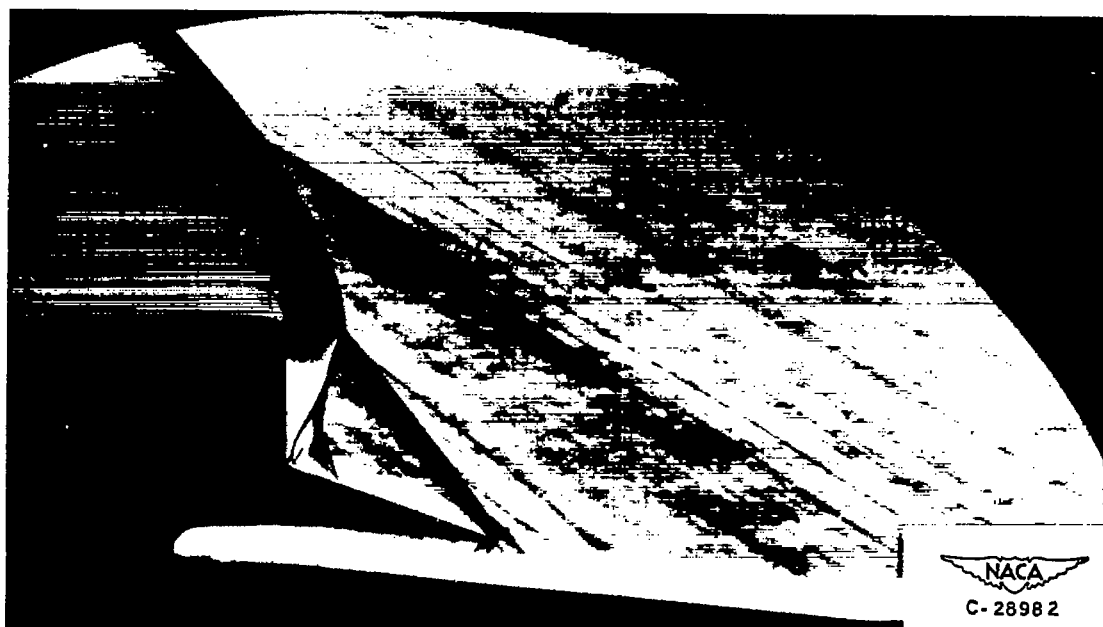


Figure 13. - Schlieren photograph of 14° -R-0.80(0) inlet at free-stream Mach number of 2.0 and angle of attack of 30° . Diffuser discharge Mach number, 0.255.

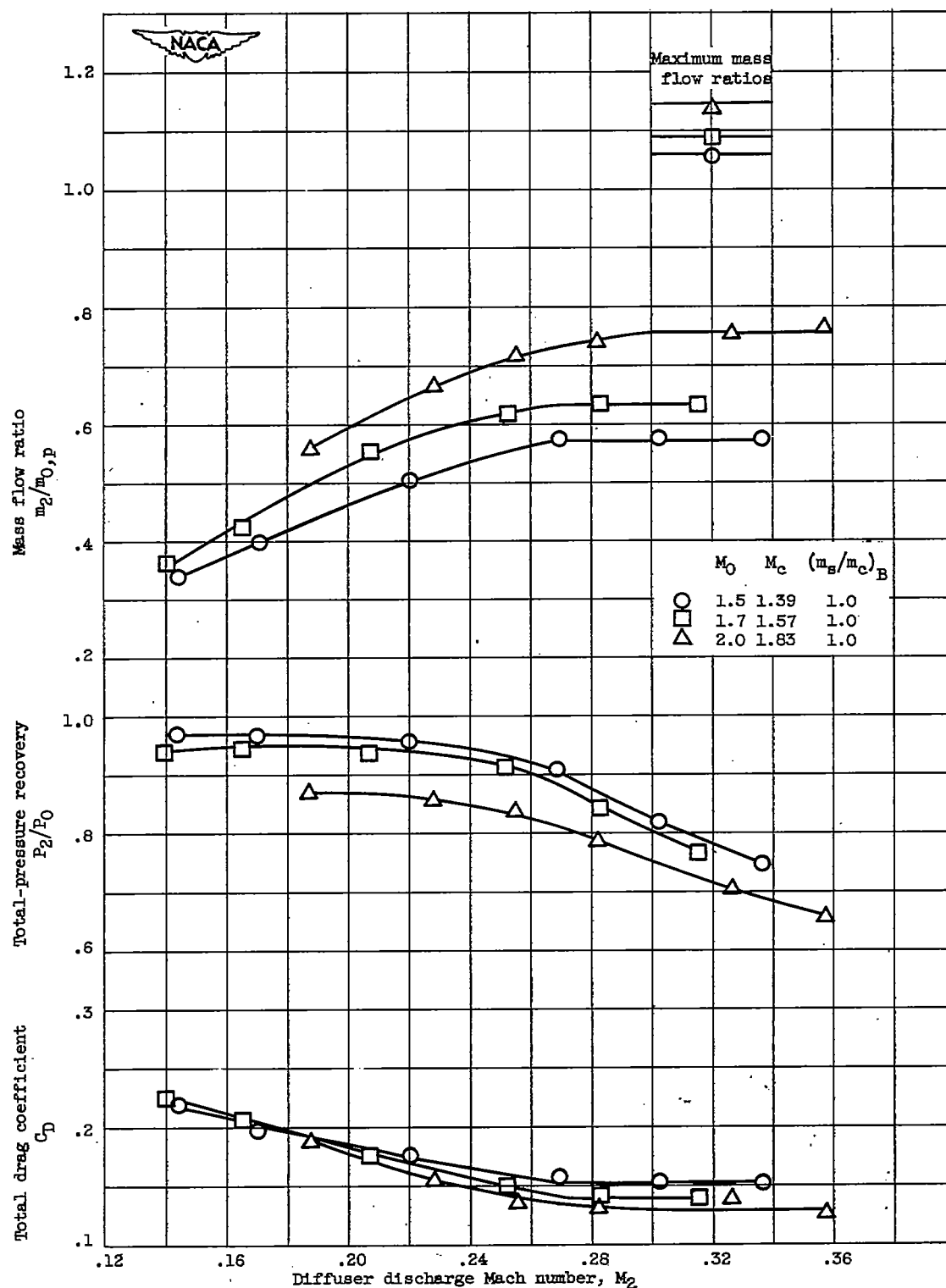


Figure 14. - Aerodynamic characteristics of 14°-R-0.80(0) inlet for range of free-stream Mach number at angle of attack of 3°.

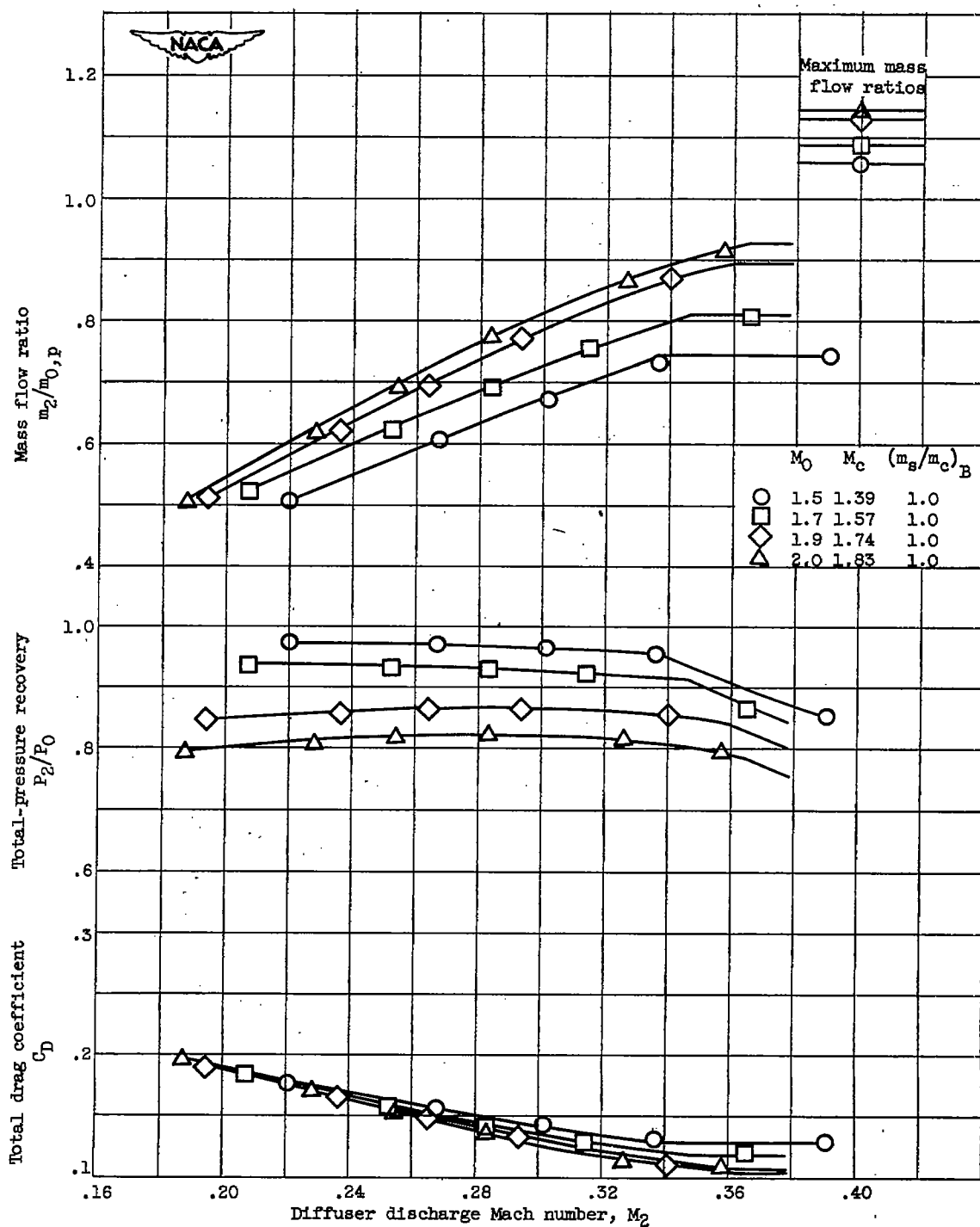


Figure 15. - Aerodynamic characteristics of 6°-R-0.80(0) inlet for range of free-stream Mach number at angle of attack of 3°.

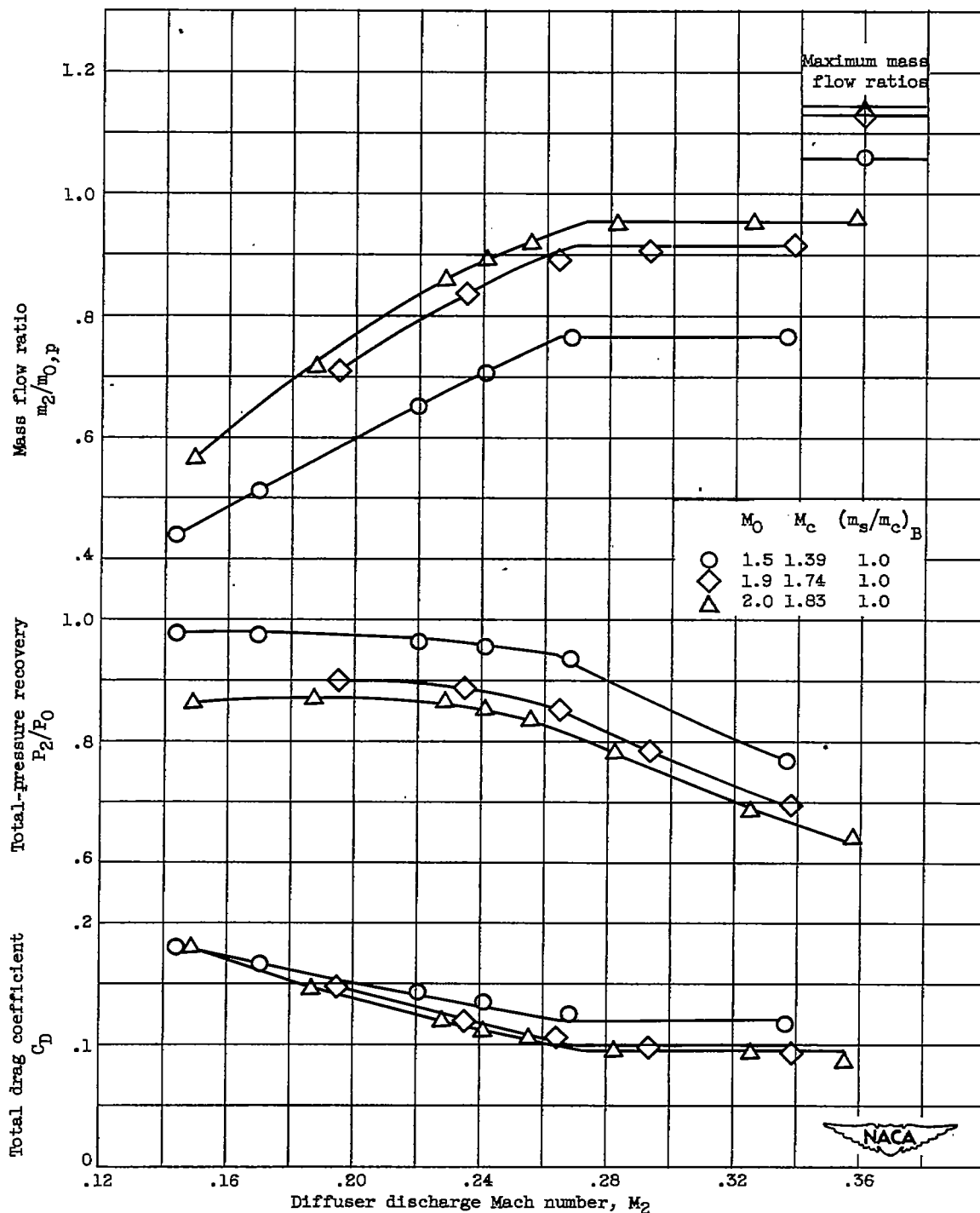


Figure 16. - Aerodynamic characteristics of 14°-8-0.80(0) inlet for range of free-stream Mach number at angle of attack of 3°.

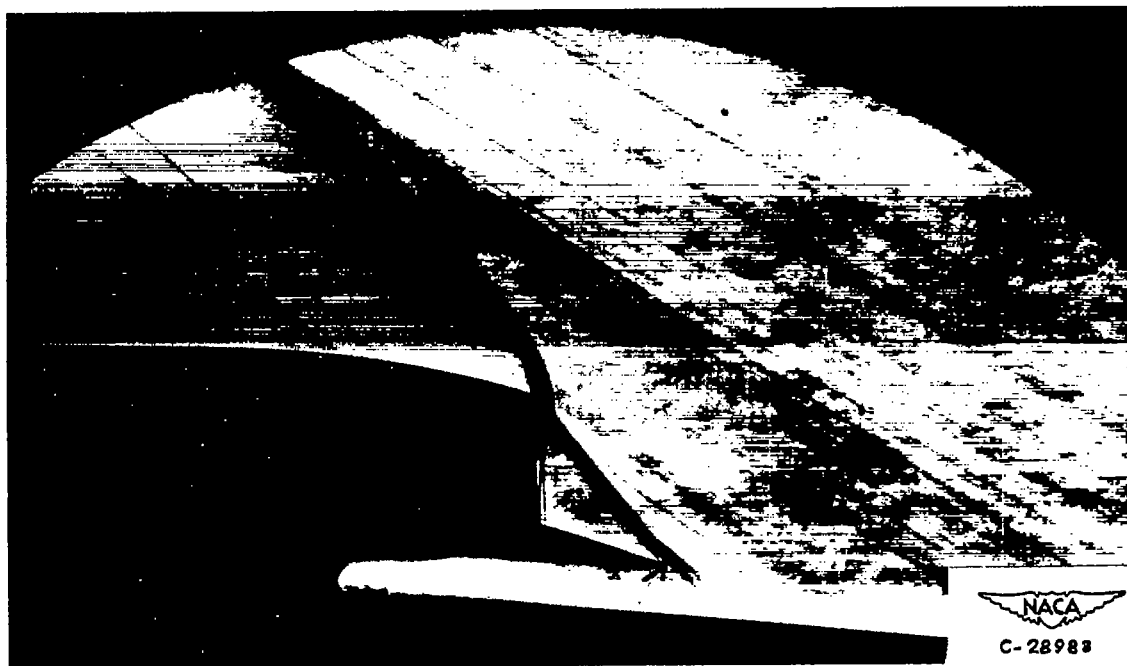


Figure 17. - Schlieren photograph of 14°-S-0.80(0) ramp inlet with extended supersonic cowl at free-stream Mach number of 2.0 and angle of attack of 3°. Diffuser discharge Mach number, 0.255.

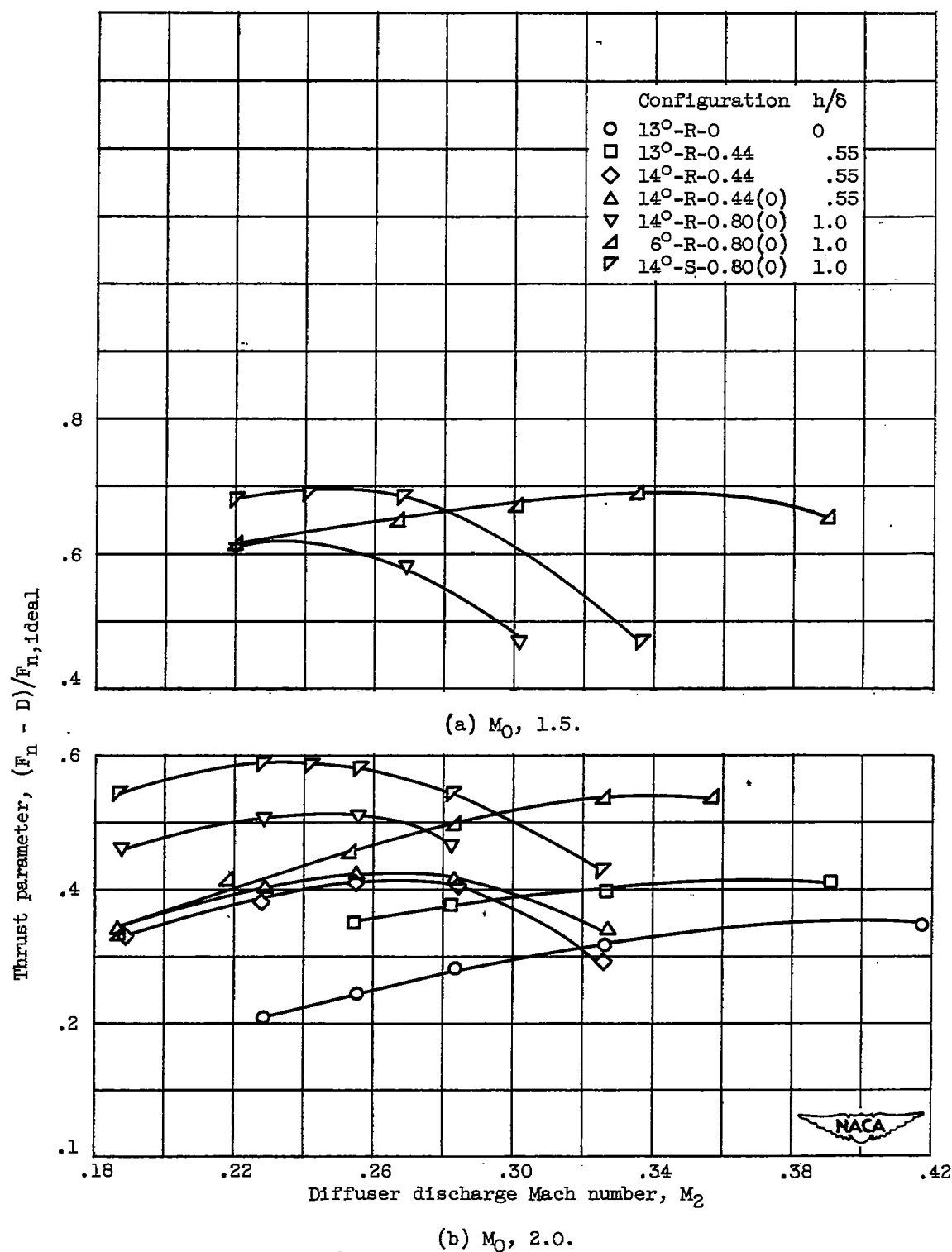


Figure 18. - Thrust parameter of inlet-engine combination at angle of attack of 3°.

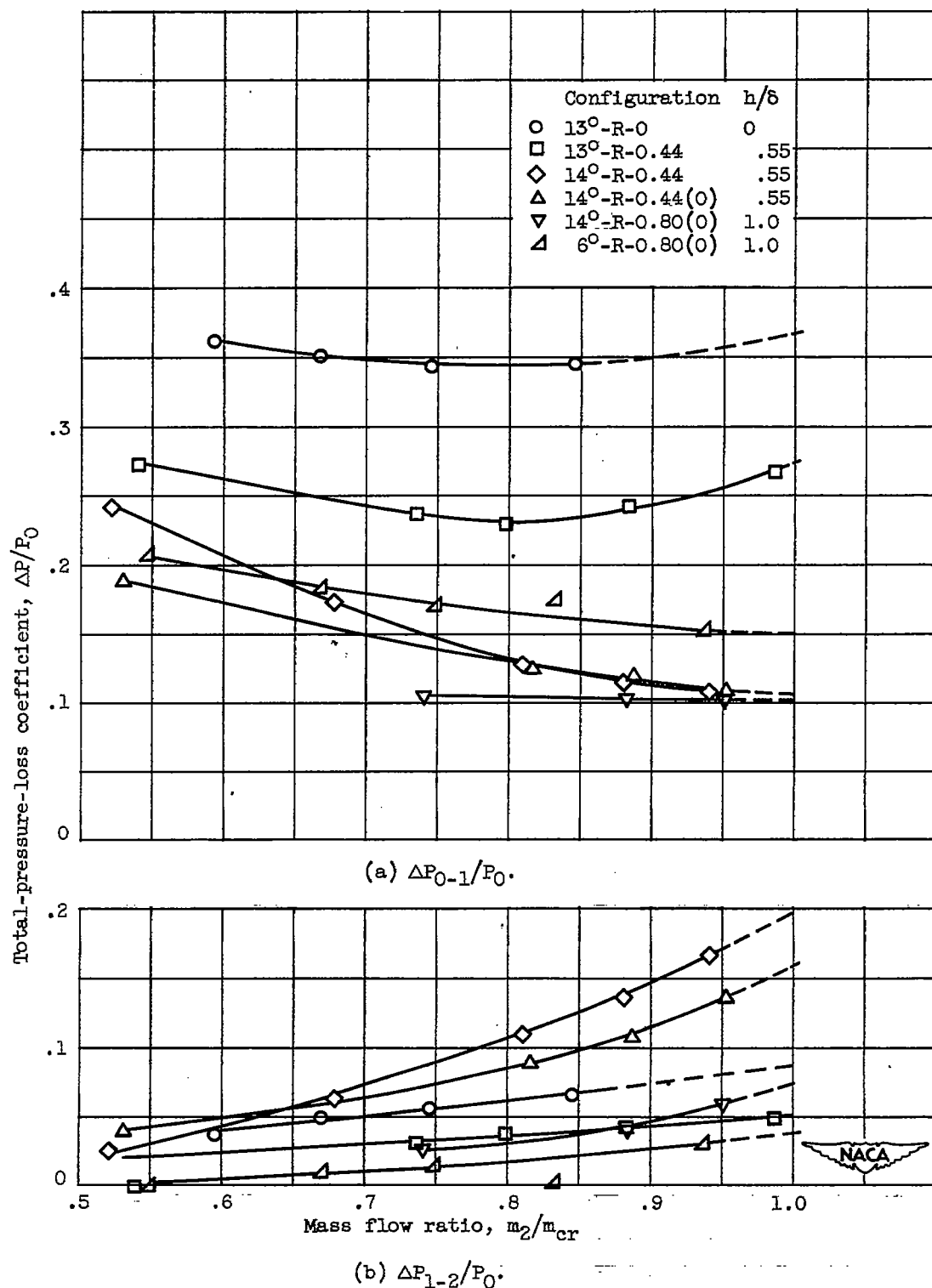


Figure 19. - Breakdown of total-pressure losses at free-stream Mach number of 2.0 and angle of attack of 3°.

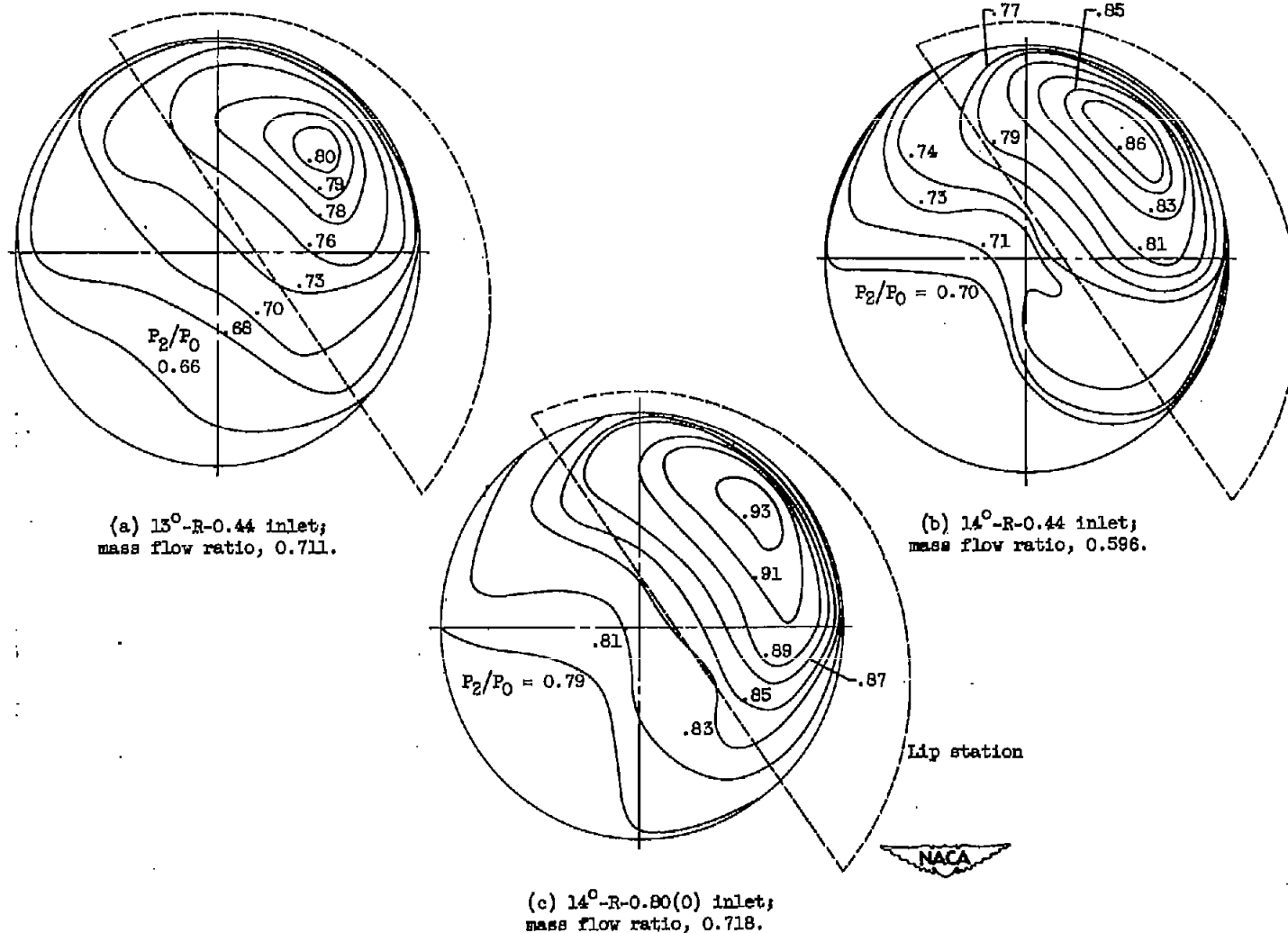


Figure 20. - Typical exit total-pressure contour maps at free-stream Mach number of 2.0 and angle of attack of 3°. Diffuser discharge Mach number, 0.255.

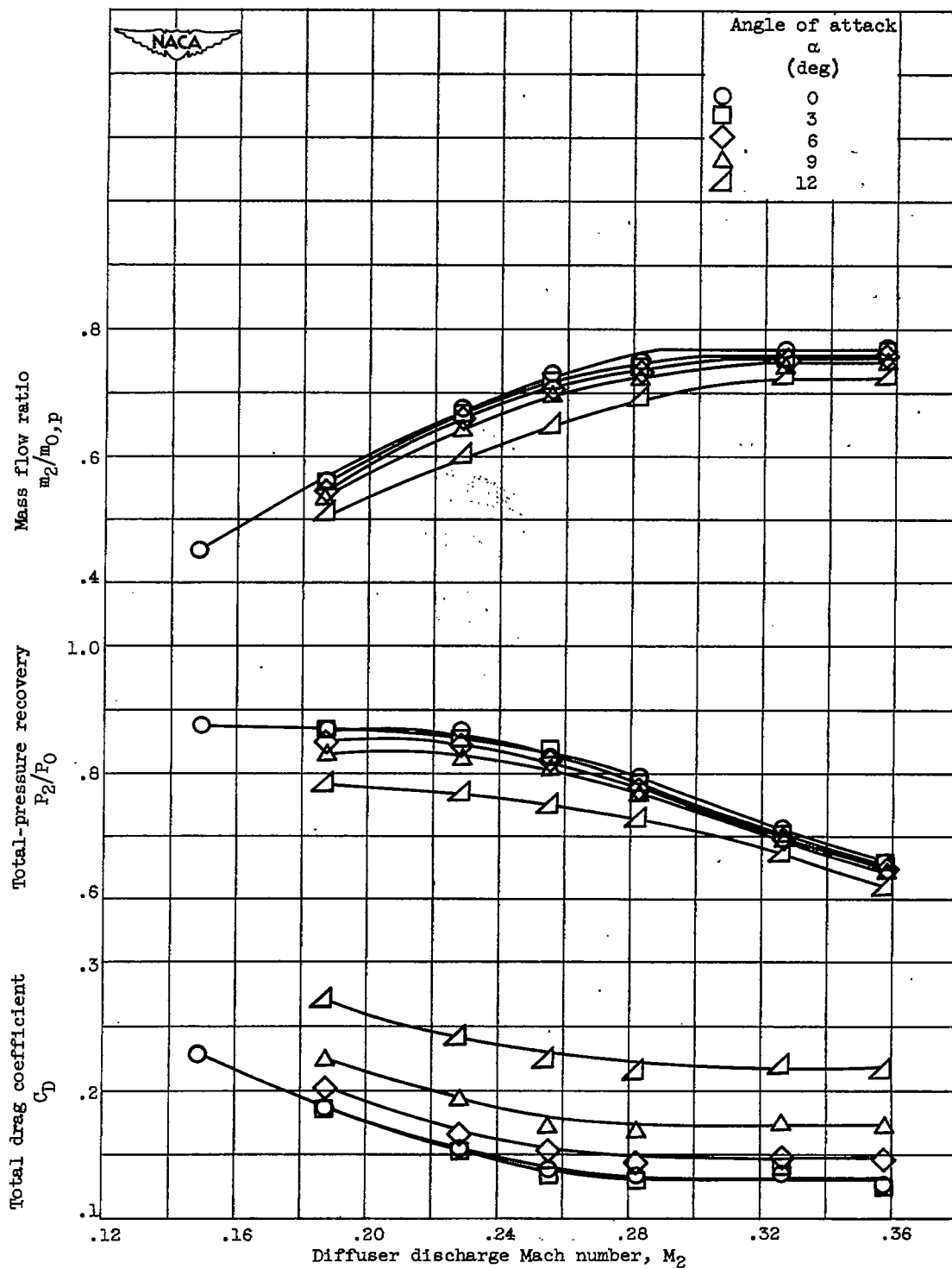


Figure 21. - Aerodynamic characteristics of 14°-R-0.80(0) inlet for range of angle of attack at free-stream Mach number of 2.0.

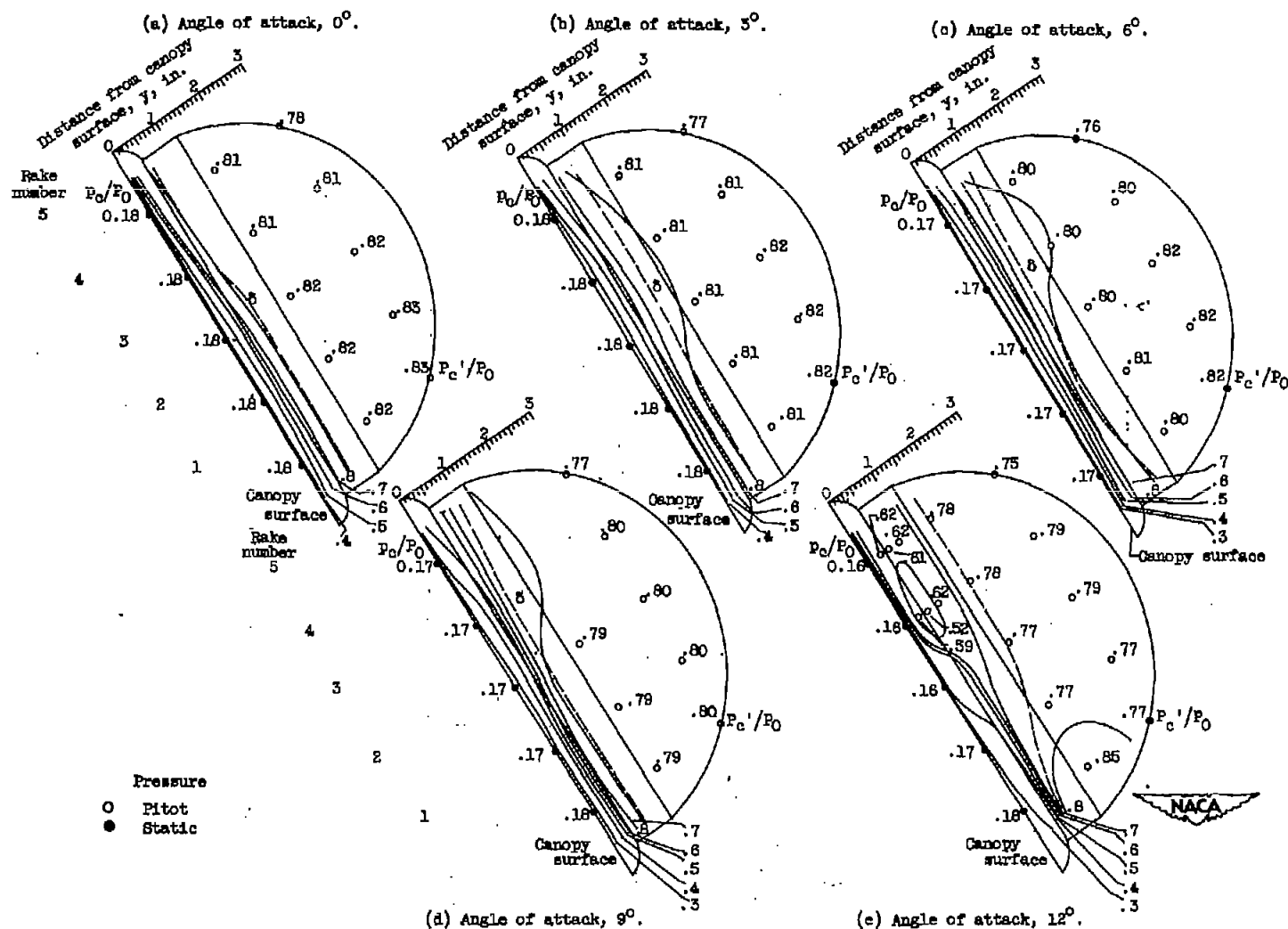
Canopy $P_c'/P_0 = 0.80$ 

Figure 22. - Pitot pressure survey upstream of inlets for range of angle of attack at free-stream Mach number of 2.0.

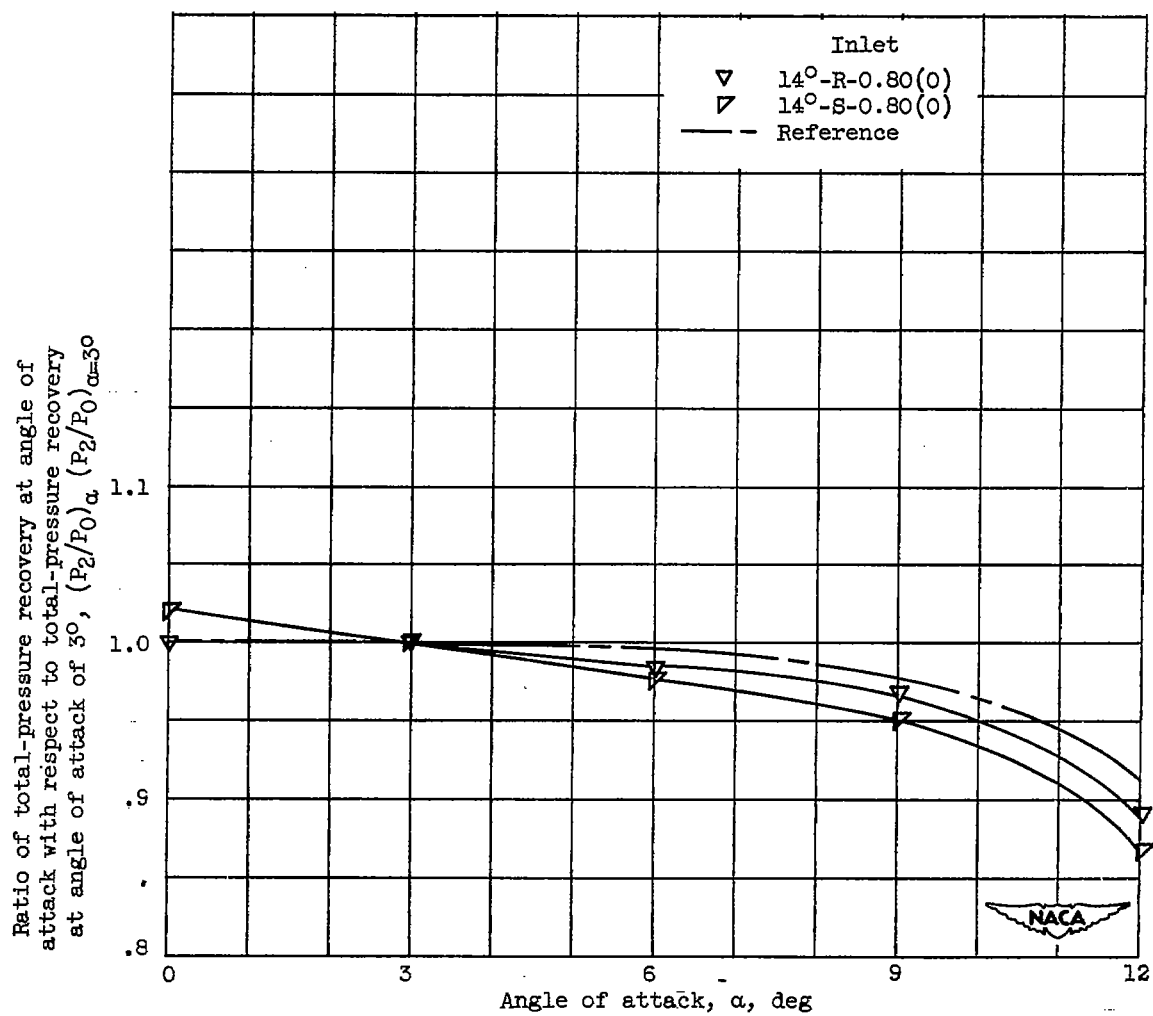


Figure 23. - Effect of change in boundary-layer thickness on total-pressure recovery at angles of attack and at free-stream Mach number of 2.0.

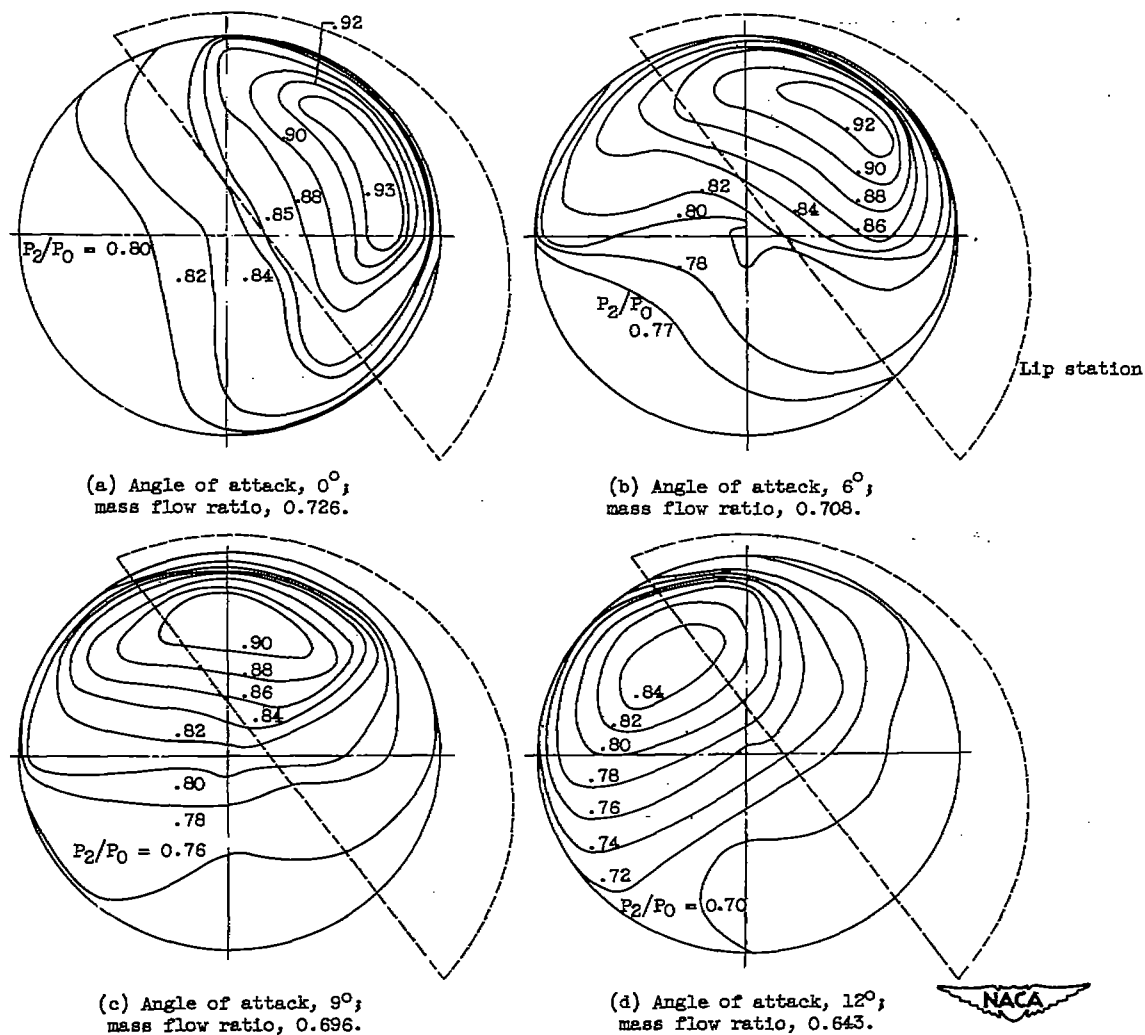


Figure 24. - Exit total-pressure contour maps of 14° -R-0.80(0) inlet for range of angle of attack at free-stream Mach number of 2.0. Diffuser discharge Mach number, 0.255 (view looking aft).

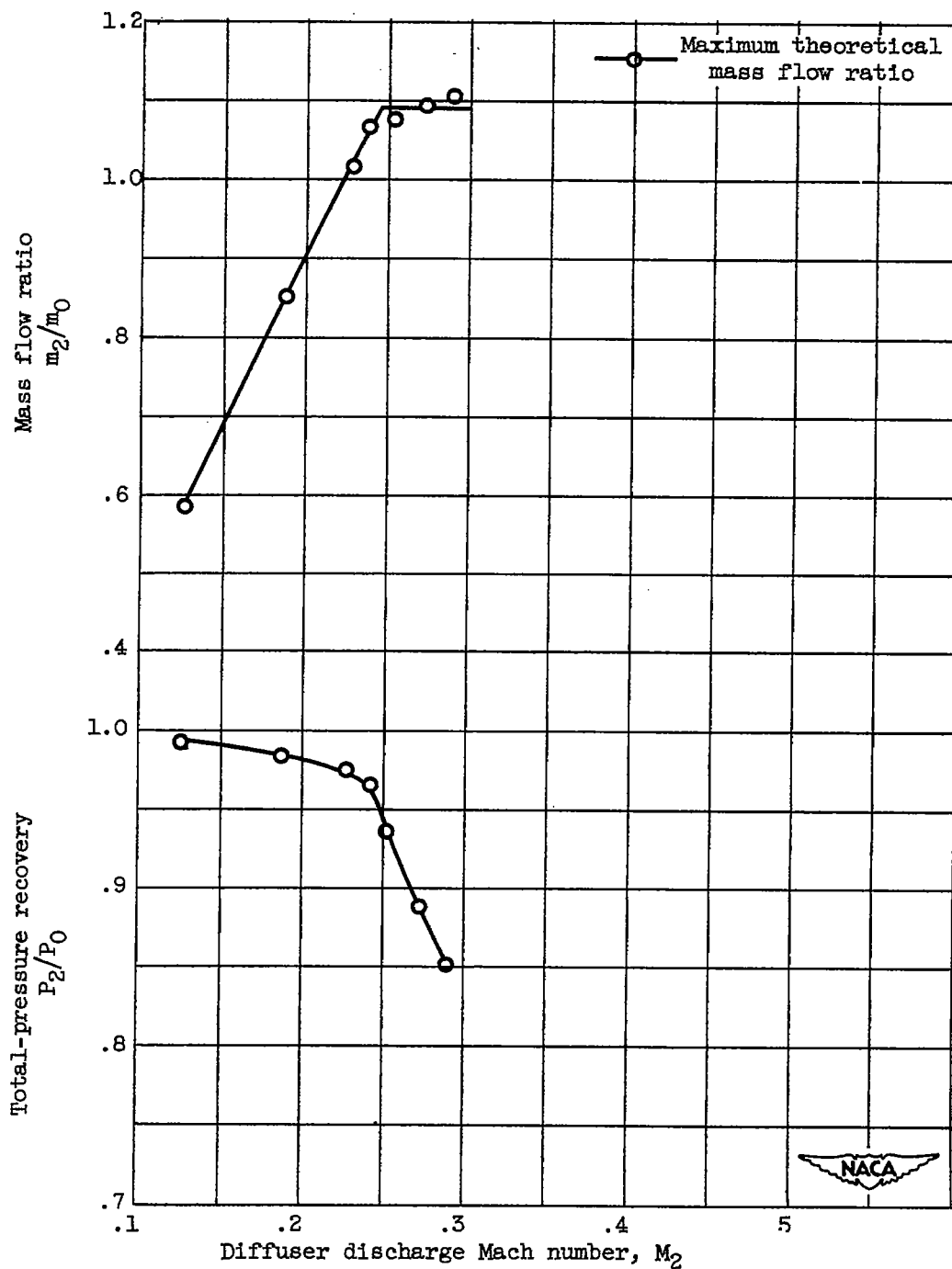


Figure 25. - Aerodynamic characteristics of $14^\circ\text{-S-0.80(0)}$ inlet with extended supersonic cowling at free-stream Mach number of 0.63 and angle of attack of 3° .

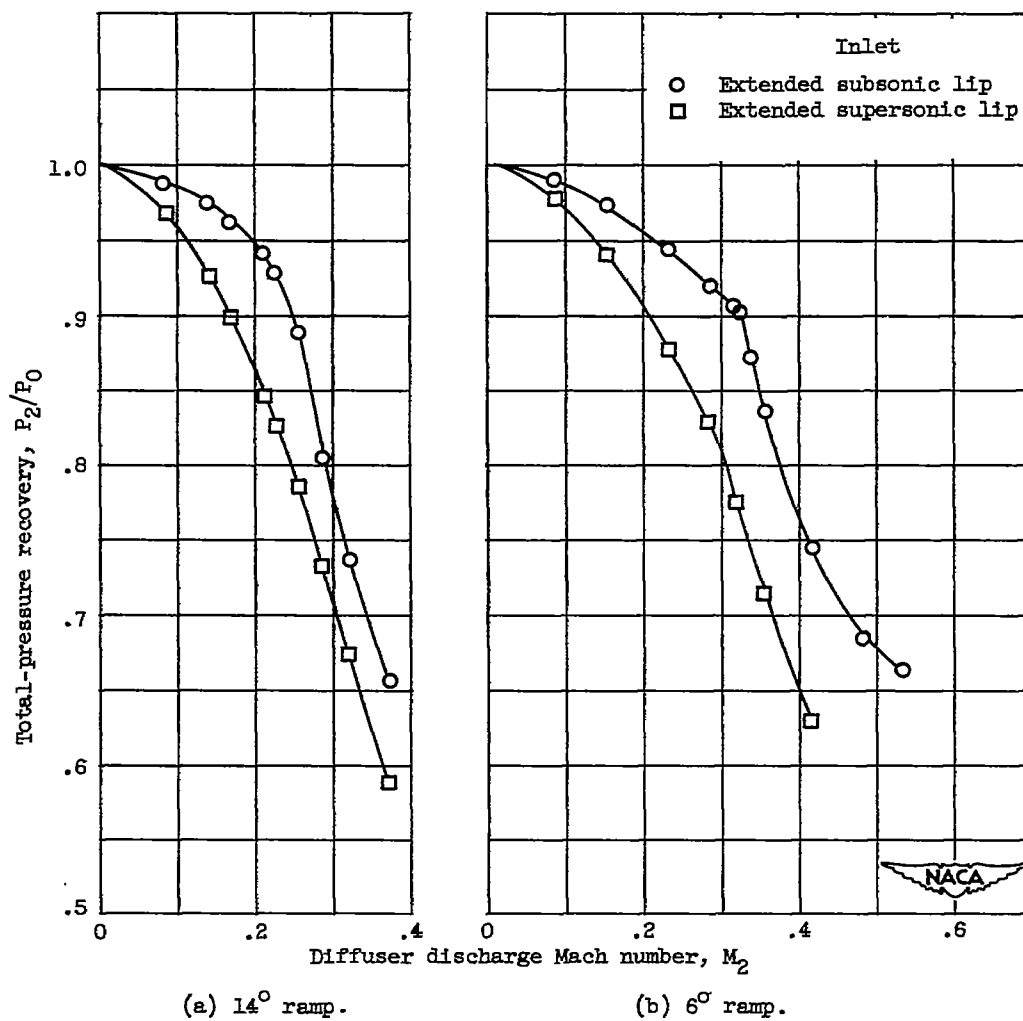


Figure 26. - Total-pressure recoveries of inlets with supersonic and subsonic cowlings at free-stream Mach number of 0.